

Parametric spin excitations in lateral quantum dots.

Jamie D. Walls^{1,*}

¹*Department of Chemistry and Chemical Biology, Harvard University, Cambridge, MA 02138*

(Dated: June 21, 2021)

In this work, the spin dynamics of a single electron under parametric modulation of a lateral quantum dot's electrostatic potential in the presence of spin-orbit coupling is investigated. Numerical and theoretical calculations demonstrate that, by squeezing and/or moving the electron's wave function, spin rotations with Rabi frequencies on the order of tens of megahertz can be achieved with experimentally accessible parameters in both parabolic and square lateral quantum dots. Applications of parametric excitations for determining spin-orbit coupling parameters and for increasing the spin polarization in the electronic ground are demonstrated.

PACS numbers:

I. INTRODUCTION

Single spin operations are an important component for possible realizations of quantum dot-based quantum computers¹. In principle, single spin manipulations can be performed using electron spin resonance (ESR) techniques with the application of oscillating magnetic fields. A recent experiment² utilizing ESR methods was used to generate spin rotations in a single electron lateral quantum dot at low static magnetic field strengths, where the required frequencies were on the order of hundreds of megahertz. However, extending ESR methods to microwave frequencies at low temperatures while minimizing the accompanying AC electric field in the semiconductor quantum dots is experimentally challenging.

Instead of considering the AC electric fields as something to be avoided, AC electric fields can be used to control the electron spin in a quantum dot. Modulations of the electrostatic potential can readily couple to the electronic degree of freedom in a semiconductor quantum dot and can be performed on the nanosecond timescale^{3,4}, which is roughly the timescale associated with the Zeeman energy in static fields on the order of a Tesla for GaAs quantum dots. However, in order to translate electronic control into spin control, there must exist an additional coupling between the spin and electronic degrees of freedom.

The two main methods of coupling the spin and electronic degrees of freedom are either through the Zeeman interaction or through spin-orbit coupling. Consider first the Zeeman interaction, which is given by $\hat{H}_Z = \vec{B}(\vec{r}) \cdot (\hat{g}(\vec{r})\mu_B\vec{S})$, where $\vec{B}(\vec{r})$ is the applied magnetic field, $\hat{g}(\vec{r})$ is the effective g-tensor, μ_B is the Bohr magneton, and \vec{S} is the electron's spin vector. Previous experimental work has demonstrated that electric fields can be used to move the electron around in the presence of a spatially dependent g-tensor, $\hat{g}(\vec{r})$, in order to generate an effective time-dependent Zeeman interaction, $\hat{H}_Z(t) = \hbar\vec{\omega}(t) \cdot \vec{S}$, which was used to perform spin rotations^{5,6}. Alternatively, $\hat{H}_Z(t)$ can also be generated by using an electric field to move an electron around in the presence of a spatially inhomogeneous magnetic field⁷.

Besides manipulating the effective Zeeman interaction, modulating the electrostatic potential can be used to manipulate the electron's spin through the spin-orbit interaction. Previous theoretical studies have proposed using electric fields to generate spin rotations via an electric dipole spin resonance (EDSR); theoretical calculations indicate that EDSR methods can be used to rotate an electron's spin on the order of tens of nanoseconds for electrons in quantum wells^{8,9,10} and quantum dots^{11,12}. For parabolic quantum dots, application of an electric field is equivalent to modulating the center of the quantum dot which, in the presence of spin-orbit coupling, is able to induce spin transitions when the modulation frequency is equal to the Zeeman frequency. Besides utilizing EDSR for spin excitation, electric fields can also be used to modulate the Rashba spin-orbit coupling constant¹³ in order to perform combined spin and orbital excitations in quantum dots¹⁴.

In this work, the spin dynamics under the combined action of spin-orbit coupling and parametric modulations of the electrostatic confining potential (such as squeezing and moving the electronic wave function) in both parabolic and square quantum dots is examined. Theoretical and numerical calculations utilizing Floquet theory and effective Hamiltonian theory are used to demonstrate that parametric modulations of the electrostatic potential can generate single spin rotations on the timescale of tens of nanoseconds using experimentally accessible parameters. In order to maximize the amplitude of the Rabi oscillations, the modulation frequency must be chosen with precision on the order of the Rabi frequency (order of 1-10 MHz). Such parametric excitations therefore can provide better energy resolution of the quantum dot's energy levels over transport measurements, where the measured energy levels are often poorly resolved due to thermal effects. Besides performing single spin rotations, we have shown that measurement of the observed Rabi oscillations^{15,16} and the required modulation frequencies can be used to determine the spin-orbit coupling parameters in the quantum dot. Finally, we have demonstrated that squeezing and expanding the electronic wave function in a parabolic quantum dot can induce both orbital and spin excitations, which can be used to increase the spin polarization of the lowest electronic state. It should be noted that relaxation is neglected throughout most of the paper since the calculated Rabi frequencies (on the order of 1-10 MHz) are at least one order of magnitude greater than the experimentally observed $1/T_1$ values found in GaAs quantum dots^{17,18,19,20}.

II. PARAMETRIC MODULATIONS AND FLOQUET THEORY

Before studying the case of parametric excitations in lateral quantum dots, the general formalism of using parametric modulations to generate excitations in quantum systems is presented. Consider a Hamiltonian which is a function of the parameter ω :

$$\begin{aligned}\widehat{H}(\omega) &= \sum_k E_k(\omega) \frac{|k(\omega)\rangle\langle k(\omega)|}{\langle k(\omega)|k(\omega)\rangle} + \sum_{j < k} \frac{\lambda_{jk}(\omega)|j(\omega)\rangle\langle k(\omega)| + \lambda_{kj}(\omega)|k(\omega)\rangle\langle j(\omega)|}{\sqrt{\langle k(\omega)|k(\omega)\rangle\langle j(\omega)|j(\omega)\rangle}} \\ &= \widehat{W}(\omega)\widetilde{H}_0(\omega)\widehat{W}^\dagger(\omega)\end{aligned}\quad (1)$$

where

$$\widetilde{H}_0(\omega) = \sum_k E_k(\omega) \frac{|k_0\rangle\langle k_0|}{\langle k_0|k_0\rangle} + \sum_{j < k} \frac{\lambda_{jk}(\omega)|j_0\rangle\langle k_0| + \lambda_{kj}(\omega)|k_0\rangle\langle j_0|}{\sqrt{\langle k_0|k_0\rangle\langle j_0|j_0\rangle}} \quad (2)$$

$$\widehat{W}(\omega) = \sum_k \frac{|k(\omega)\rangle\langle k_0|}{\sqrt{\langle k(\omega)|k(\omega)\rangle\langle k_0|k_0\rangle}} \quad (3)$$

with $|k_0\rangle \equiv |k(\omega_0)\rangle$. The transformation $\widehat{W}(\omega)$ simply switches from the basis $\{|k(\omega_0)\rangle\}$ to the basis $\{|k(\omega)\rangle\}$.

In order to induce transitions between two arbitrary states $|k(\omega)\rangle$ and $|j(\omega)\rangle$ efficiently, the matrix element coupling these states must be modulated at a frequency ω_r given by $n\hbar\omega_r \approx |E_j(\omega) - E_k(\omega)|$ for integer n . The time-dependent coupling between states can in principle be generated by modulating the parameter ω of $\widehat{H}(\omega)$. The propagator during modulation of ω can be written as:

$$\begin{aligned}\widehat{U}(t) &= T \exp\left(-\frac{i}{\hbar} \int_0^t dt' \widehat{H}(\omega(t'))\right) \\ &= T \exp\left(-\frac{i}{\hbar} \int_0^t dt' \widehat{W}(\omega(t'))\widetilde{H}_0(\omega(t'))\widehat{W}^\dagger(\omega(t'))\right) \\ &= \widehat{W}(\omega(t))T \exp\left(-\frac{i}{\hbar} \int_0^t dt' \left[-i\hbar\widehat{W}^\dagger(\omega(t'))\frac{\partial\widehat{W}(\omega(t'))}{\partial t'} + \widetilde{H}_0(\omega(t'))\right]\right) \\ &= \widehat{W}(\omega(t))T \exp\left(-\frac{i}{\hbar} \int_0^t dt' \widetilde{H}(t')\right)\end{aligned}\quad (4)$$

where

$$\widetilde{H}(t) = \widetilde{H}_0(\omega(t)) - i\hbar\widehat{W}^\dagger(\omega(t))\frac{\partial\widehat{W}(\omega(t))}{\partial t} \quad (5)$$

$$-i\hbar\widehat{W}^\dagger(\omega(t))\frac{\partial\widehat{W}(\omega(t))}{\partial t} = \left(\sum_k V_{kk}(t) \frac{|k_0\rangle\langle k_0|}{\langle k_0|k_0\rangle} + \sum_{j < k} \frac{V_{jk}(t)|j_0\rangle\langle k_0| + V_{kj}(t)|k_0\rangle\langle j_0|}{\sqrt{\langle j_0|j_0\rangle\langle k_0|k_0\rangle}}\right) \quad (6)$$

with

for $j \neq k$

$$\begin{aligned}V_{kj}(t) &= -i\hbar \frac{\partial\omega(t)}{\partial t} \frac{\langle k(\omega(t))|\frac{\partial j(\omega(t))}{\partial\omega(t)}\rangle}{\sqrt{\langle j(\omega(t))|j(\omega(t))\rangle\langle k(\omega(t))|k(\omega(t))\rangle}} \\ &= -\frac{i\hbar}{\Delta_{jk}(\omega(t))} \frac{\partial\omega(t)}{\partial t} \frac{\langle k(\omega(t))|\frac{\partial\widehat{H}(\omega(t))}{\partial\omega(t)}|j(\omega(t))\rangle}{\sqrt{\langle j(\omega(t))|j(\omega(t))\rangle\langle k(\omega(t))|k(\omega(t))\rangle}}\end{aligned}\quad (7)$$

for $j = k$

$$V_{kk}(t) = -i\hbar \frac{\partial\omega(t)}{\partial t} \frac{\langle k(\omega(t))|\frac{\partial k(\omega(t))}{\partial\omega(t)}\rangle}{\langle k(\omega(t))|k(\omega(t))\rangle} \quad (8)$$

where $\Delta_{jk}(\omega(t)) = E_j(\omega(t)) - E_k(\omega(t))$. Note that $\int_0^t dt' V_{kk}(t')/\hbar$ is just the geometric phase²¹ associated with the parametric modulation of $\widehat{H}(\omega)$.

In the following, we are interested in the case where only small, periodic modulations to ω are performed, i.e., $\omega(t) = \omega + \delta\omega \sin(\omega_r t + \phi)$ where $\delta\omega \ll \omega$, and ω_r and ϕ are the modulation frequency and the initial phase respectively. If the energy difference between the states $|j_0\rangle$ and $|k_0\rangle$ is much greater than the generated off-diagonal matrix elements ($|\Delta_{jk}(\omega(0))| \gg |V_{jk}|$), then the two states will remain uncoupled unless $|\Delta_{jk}(\omega(0))|$ is equal to a multiple of $\hbar\omega_r$, i.e., $n\hbar\omega_r \approx |\Delta_{jk}(\omega(0))|$ where n is an integer. In order to gain insight into the dynamics under periodic modulation of the Hamiltonian, Floquet theory²² can be used to solve for $\hat{U}(t)$ in Eq. (4). Rewriting $\tilde{H}(t)$ in Eq. (5) as $\tilde{H}(t) = \tilde{H}_0(\omega(0)) + \hat{V}(t)$, with $\tilde{H}_0(\omega(0))$ given by Eq. (3) and $\hat{V}(t) = \sum_m \hat{V}_m \exp(im\omega_r t)$, the effective propagator can be written as:

$$\hat{W}^\dagger(t)\hat{U}(t) = T \exp\left(-\frac{i}{\hbar} \int_0^t dt' \tilde{H}(t')\right) \quad (9)$$

$$= T \exp\left(-\frac{i}{\hbar} \int_0^t dt' \left[\tilde{H}_0(\omega(0)) + \sum_m \hat{V}_m \exp(im\omega_r t)\right]\right) \\ = \sum_{n=-\infty}^{\infty} \exp(in\omega_r t) \hat{U}_n(t) \quad (10)$$

where Eq. (10) represents the Fourier decomposition of the propagator $\hat{U}(t)$ into the Fourier operators, $\hat{U}_n(t)$, which satisfy:

$$\frac{d\hat{U}_n(t)}{dt} = -\frac{i}{\hbar} \left(n\omega_r \hat{1} + \tilde{H}_0(\omega(0))\right) \hat{U}_n(t) - \frac{i}{\hbar} \sum_m \hat{V}_m \hat{U}_{n-m}(t) \quad (11)$$

with the initial conditions chosen to be $\hat{U}_0(0) = \hat{1}$ and $\hat{U}_{n \neq 0} = \hat{0}$ in order that $\hat{U}(0) = \hat{1}$. The solution to Eq. (11) is given by $\hat{U}(t) = \exp(-i\hat{H}_F t/\hbar) \hat{U}(0)$, where $\hat{U}(t)$ can be formally represented as a vector in Floquet space, $\hat{U}(t) = \sum_{n=-\infty}^{\infty} \hat{U}_n(t) |n_F\rangle$ with $\hat{U}(0) = \hat{1} |0_F\rangle$ [where the various Floquet states $|n_F\rangle$ satisfy $\langle n_F | m_F \rangle = \delta_{n_F, m_F}$], and $U_n(t) = \langle n_F | \exp(-i\hat{H}_F t/\hbar) | 0_F \rangle$. The time-independent Floquet Hamiltonian, \hat{H}_F , is defined by:

$$\langle n_F | \hat{H}_F | m_F \rangle = \langle n_F | \tilde{H}_{0,F} + \hat{N}_F \hbar\omega_r | m_F \rangle + \langle n_F | \hat{V}_F | m_F \rangle \\ = \delta_{n_F, m_F} \left(\tilde{H}_0(\omega(0)) + n_F \hbar\omega_r \hat{1} \right) + \sum_k \delta_{n_F - k, m_F} \hat{V}_k \quad (12)$$

where the states in Floquet space are denoted by $|j, n_F\rangle$, with $(\tilde{H}_{0,F} + \hat{N}_F \hbar\omega_r) |j, n_F\rangle = (E_j(\omega(0)) + n_F \hbar\omega_r) |j, n_F\rangle$.

By going into Floquet space, the initial time-dependent Hamiltonian, $\tilde{H}(t)$, has been replaced by the time-independent Floquet Hamiltonian, \hat{H}_F ; however, in order to calculate $\hat{U}(t)$, we must now exponentiate \hat{H}_F , which is an infinite dimensional matrix in Floquet space, since $\langle n_F | \hat{H}_F | m_F \rangle$ is defined for all $n_F, m_F \in \{-\infty, \infty\}$. However, the propagator can be simplified if there exists a finite dimensional subspace of nearly degenerate states, Q , which is weakly coupled to states outside of Q . In this case, the dynamics within Q can be separated from the rest of the Floquet space by constructing an effective Hamiltonian^{23,24} within the subspace Q by treating the coupling to states outside of Q perturbatively. For example, take $Q = \{|j, n_F\rangle, |k, (n+p)_F\rangle\}$ with $E_j(\omega(0)) \approx E_k(\omega(0)) + p\hbar\omega_r$, and assume that Q is weakly coupled to states outside of Q (i.e., $|\langle j, n_F | \hat{V}_F | q, m_F \rangle| \ll |E_j(\omega(0)) - E_q(\omega(0)) + (n-m)_F \hbar\omega_r|$ and $|\langle k, (n+p)_F | \hat{V}_F | q, m_F \rangle| \ll |E_k(\omega(0)) - E_q(\omega(0)) + (n+p-m)_F \hbar\omega_r|$), an effective Hamiltonian can be written in the subspace Q by using a unitary transformation, $\exp(\hat{S}_F)$, where $\exp(\hat{S}_F) \hat{H}_F \exp(-\hat{S}_F) = \hat{H}_F^{\text{EFF}}$; the state $|j, n_F\rangle$ is only coupled to the state $|k, (n+p)_F\rangle$ in \hat{H}_F^{EFF} , i.e., $\langle p, r_F | \hat{H}_F^{\text{EFF}} | m, q_F \rangle \neq 0$ only if $|m, q_F\rangle, |p, r_F\rangle \in Q$. A perturbation series for \hat{S}_F in powers of \hat{V}_F , $\hat{S}_F = \sum_{n=1}^{\infty} \hat{S}_F^{(n)}$, can be constructed and is given in Appendix A.

Using \hat{H}_F^{EFF} , the propagator, $\hat{U}(t)$ can finally be written as:

$$\hat{W}^\dagger(t)\hat{U}(t) = \sum_{n=-\infty}^{\infty} \exp(in\omega_r t) U_n(t) \\ = \sum_{n=-\infty}^{\infty} \exp(in\omega_r t) \langle n_F | \exp(-\hat{S}_F) \exp\left(-\frac{i}{\hbar} \hat{H}_F^{\text{EFF}} t\right) \exp(\hat{S}_F) | 0_F \rangle \\ \approx \sum_{n=-\infty}^{\infty} \exp(in\omega_r t) \left(\langle n_F | \exp\left(-\frac{i}{\hbar} \hat{H}_F^{\text{EFF}} t\right) | 0_F \rangle - \langle n_F | [\hat{S}_F^{(1)}, \exp\left(-\frac{i}{\hbar} \hat{H}_F^{\text{EFF}} t\right)] | 0_F \rangle \right) \quad (13)$$

The resulting propagator, projected onto the $\{|j_0\rangle, |k_0\rangle\}$ subspace (where $\widehat{P}_s = |j_0\rangle\langle j_0| + |k_0\rangle\langle k_0|$), is given by:

$$\widehat{P}_s \widehat{W}^\dagger(t) \widehat{U}(t) \widehat{P}_s = \widehat{Z}(\omega_r t) \left(\widehat{U}^{jk}(t) - \sum_{n \neq 0} \exp(in\omega_r t) \widehat{X}_n \widehat{U}^{jk}(t) - \widehat{U}^{jk}(t) \widehat{X}_n \right) \quad (14)$$

where

$$\widehat{X}_n = \begin{pmatrix} \frac{\langle j, n_F | \widehat{V}_F | j, 0_F \rangle}{n\omega_r} & \frac{\langle j, (n-p)_F | \widehat{V}_F | k, 0 \rangle}{\Delta_{jk} + (n-p)\hbar\omega_r} \\ \frac{\langle k, (n+p)_F | \widehat{V}_F | j, 0 \rangle}{(n+p)\hbar\omega_r - \Delta_{jk}} & \frac{\langle k, n_F | \widehat{V}_F | k, 0_F \rangle}{n\omega_r} \end{pmatrix}$$

$$\widehat{Z}(\omega_r t) = \begin{pmatrix} 1 & 0 \\ 0 & \exp(i\omega_r t) \end{pmatrix} \quad (15)$$

and $\widehat{U}^{jk}(t) = \exp(-i\widehat{H}_{\text{EFF}}^{jk}t/\hbar)$, where $\widehat{H}_{\text{EFF}}^{jk}$ is the effective Hamiltonian in the $\{|j, 0_F\rangle, |k, p_F\rangle\}$ Floquet subspace, i.e., $\widehat{H}_{\text{EFF}}^{jk} = (|j, 0_F\rangle\langle j, 0_F| + |k, p_F\rangle\langle k, p_F|) \widehat{H}_F^{\text{EFF}} (|j, 0_F\rangle\langle j, 0_F| + |k, p_F\rangle\langle k, p_F|)$.

III. PARAMETRIC MODULATIONS IN LATERAL, PARABOLIC QUANTUM DOTS

Using the formalism presented in Section II, we are now ready to begin studying parametric excitation in a single-electron, lateral quantum dot, which is taken to lie in the XY plane with the electron's wave function strongly confined along the \widehat{z} direction. In the following, only an in-plane magnetic field, $\vec{B} = B \cos(\theta)\widehat{x} + B \sin(\theta)\widehat{y}$, will be considered, which allows one to neglect orbital effects associated with an out of plane magnetic field. The Hamiltonian for a single-electron lateral quantum dot defined by the electrostatic potential $\widehat{V}(\widehat{X}, \widehat{Y})$, in the presence of spin-orbit coupling (for the moment, only Rashba²⁵ and linear Dresselhaus²⁶ are considered), is given by:

$$\widehat{H} = \widehat{H}_0 + \widehat{H}_{SO} \quad (16)$$

$$\widehat{H}_0 = \frac{\widehat{P}_X^2}{2m^*} + \frac{\widehat{P}_Y^2}{2m^*} + \widehat{V}(\widehat{X}, \widehat{Y}) - \frac{\hbar\omega_Z}{2} \widehat{\sigma}_Z \quad (17)$$

$$\widehat{H}_{SO} = \frac{\widehat{P}_X}{\hbar} (\zeta_1(-\theta)\widehat{\sigma}_X + \zeta_2(\theta)\widehat{\sigma}_Z) - \frac{\widehat{P}_Y}{\hbar} (\zeta_2(-\theta)\widehat{\sigma}_X + \zeta_1(\theta)\widehat{\sigma}_Z) \quad (18)$$

where $\hbar\omega_Z = |g\mu_B \vec{B}|$, $\zeta_1(\theta) = \alpha \cos(\theta) - \beta \sin(\theta)$, $\zeta_2(\theta) = \alpha \sin(\theta) - \beta \cos(\theta)$ [where α and β are the Rashba and linear Dresselhaus coupling constants respectively], and the vector potential, $\vec{A} = \widehat{Z} \sin(\theta)\widehat{x} - \widehat{Z} \cos(\theta)\widehat{y}$, was chosen. Due to the strong confinement along the \widehat{z} -direction, all terms linear in \widehat{Z} have been truncated/removed from \widehat{H} in Eqs. (16)-(18), with terms quadratic in \widehat{Z} being incorporated into the the confining potential along the \widehat{z} -direction. The electrostatic potential, $\widehat{V}(\widehat{X}, \widehat{Y})$, mostly results from voltages applied to surface gates above the 2DEG, which confines the electron within the quantum dot; changing the voltages of the surface gates can change $\widehat{V}(\widehat{X}, \widehat{Y})$. The spin quantization axis has been taken to be along the direction of the in-plane magnetic field. The eigenstates of \widehat{H}_0 are denoted by $|n, \pm\rangle$, where $\widehat{H}_0|n, \pm\rangle = (E_n \mp \hbar\omega_Z/2)|n, \pm\rangle$. In the presence of spin-orbit coupling, the various $|n, \pm\rangle$ states are mixed; however, if the confinement strength is much larger than the spin-orbit coupling strength, i.e., $|\langle n, \pm | \widehat{H}_{SO} | m, \pm \rangle| \ll |\Delta_{nm}|$ and $|\langle n, \mp | \widehat{H}_{SO} | m, \pm \rangle| \ll |\Delta_{nm} \pm \omega_Z|$ for all n and m , \widehat{H}_{SO} is suppressed and can be treated as a perturbation to \widehat{H}_0 .

In this section, a lateral quantum dot defined by a parabolic electrostatic potential will be examined. Such parabolic potentials have enjoyed tremendous success in describing transport and spectral properties in lateral quantum dots^{27,28,29}. The electrostatic potential for a parabolic quantum dot can be written as:

$$\begin{aligned} \widehat{V}(\widehat{X}, \widehat{Y}) &= \frac{m^*\omega_X^2}{2} (\widehat{X} - x_{c'})^2 + \frac{m^*\omega_Y^2}{2} (\widehat{Y} - y_{c'})^2 - eF_X \widehat{X} - eF_Y \widehat{Y} \\ &= \frac{m^*\omega_X^2}{2} \left(\widehat{X} - \frac{eF_X}{m^*\omega_X^2} - x_{c'} \right)^2 + \frac{m^*\omega_Y^2}{2} \left(\widehat{Y} - \frac{eF_Y}{m^*\omega_Y^2} - y_{c'} \right)^2 - \frac{e^2 F_X^2}{2m^*\omega_X^2} - \frac{e^2 F_Y^2}{2m^*\omega_Y^2} \end{aligned} \quad (19)$$

where $\vec{r}_{c'} = x_{c'}\widehat{x} + y_{c'}\widehat{y}$ is the center of the parabolic well, ω_X and ω_Y are the oscillator frequencies of the parabolic dot, and F_X and F_Y are static electric fields which do not alter the energy levels of the quantum dot but do shift the effective center of the quantum dot to $\vec{r}_c = [x_{c'} + eF_X/(m^*\omega_X^2)]\widehat{x} + [y_{c'} + eF_Y/(m^*\omega_Y^2)]\widehat{y}$. For convenience, $\widehat{V}(\widehat{X}, \widehat{Y})$

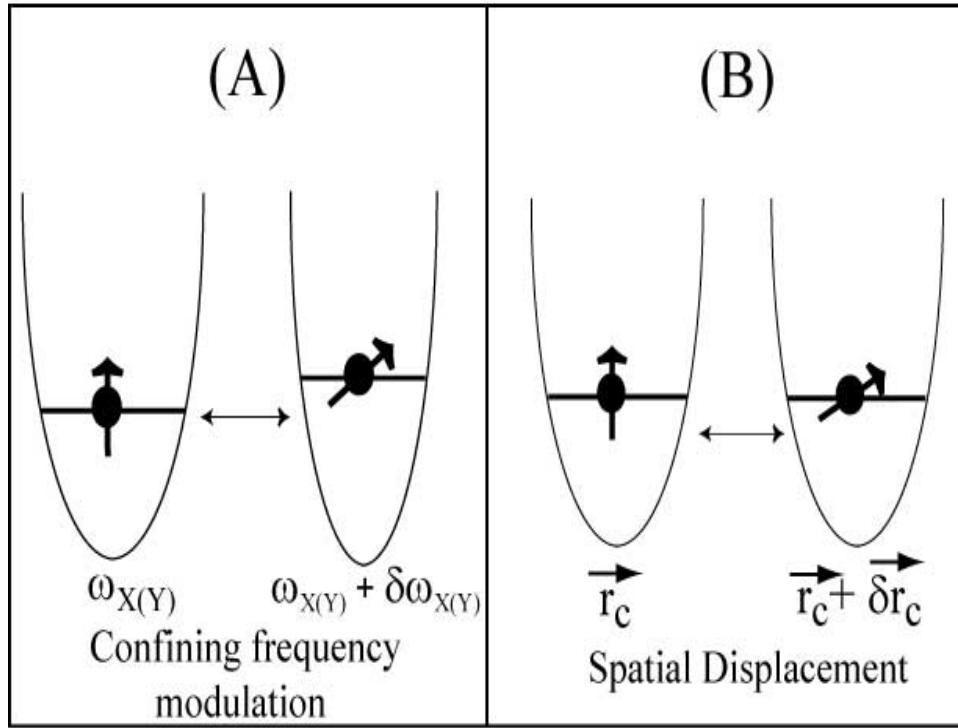


FIG. 1: Parametric modulations of a parabolic quantum dot's confining potential by either modulating (A) the confining frequency (ω_X and/or ω_Y) or (B) the center of the dot, $\vec{r}_c = x_c\hat{x} + y_c\hat{y}$. In the presence of spin-orbit coupling, if either $\delta\omega_{X(Y)}(t)$ or $\delta\vec{r}_c(t) \equiv \delta x_c(t)\hat{x} + \delta y_c(t)\hat{y}$ is modulated at roughly the energy difference between $|0, 0, +\rangle$ and $|0, 0, -\rangle$, effective spin rotations can be performed as depicted in Fig. 1.

in Eq. (19) was taken to be separable in the \hat{X} and \hat{Y} degrees of freedom; that is, the principal axes of $\hat{V}(\hat{X}, \hat{Y})$ were chosen for convenience to be the same as those used in Eq. (16) (if this is not the case, inclusion of terms like $\lambda\hat{X}\hat{Y}$ can be readily incorporated into the following theory). The eigenstates of \hat{H}_0 for parabolic confinement, $|n, m, \pm\rangle$, satisfy $\hat{H}_0|n, m, \pm\rangle = [\hbar\omega_X(n + 1/2) + \hbar\omega_Y(m + 1/2) \mp \hbar\omega_Z/2]|n, m, \pm\rangle$ and are centered about \vec{r}_c . Under conditions of strong confinement (where $\hbar\omega_X, \hbar\omega_Y \gg |\hat{H}_{SO}|$), the states $|0, 0, +\rangle$ and $|0, 0, -\rangle$ are approximately the two lowest energy eigenstates. Transitions between these two states correspond to spin rotations within the ground electronic state.

As discussed in Section II, efficient transitions between the states $|0, 0, +\rangle$ and $|0, 0, -\rangle$ in the quantum dot can occur whenever the Hamiltonian is parametrically modulated at roughly the energy difference between the two states. There are two natural modulation parameters to choose from in parabolic quantum dot potentials as shown in Fig. 1: either modulation of the oscillator frequencies [$\omega_{X(Y)} \rightarrow \omega_{X(Y)} + \delta\omega_{X(Y)}$ in Fig. 1(A)], or modulation of the center of the quantum dot [$\vec{r}_c \rightarrow \vec{r}_c + \delta\vec{r}_c$ in Fig. 1(B)] (note that modulation of F_X and/or F_Y is equivalent to modulating \vec{r}_c). Such parametric modulations can in principle be performed by modulating the surface gate voltages which define $\hat{V}(\hat{X}, \hat{Y})$. Modulations of surface gate voltages have been experimentally performed on the nanosecond timescale^{3,4}.

A. Parametric Modulations of the Confining Strength in a Parabolic Quantum Dot

The modulation the the oscillator strengths of the quantum dot, $\omega_{X(Y)} \rightarrow \omega_{X(Y)}(t) = \omega_{X(Y)} + \delta\omega_{X(Y)}(t)$, corresponds to squeezing and expanding the electron's wave function in a time-dependent manner, as illustrated in Fig. 1(A). Using Eq. (4), the

effective time-dependent Hamiltonian during modulation of ω_X and ω_Y at a frequency ω_r is given by:

$$\begin{aligned} \frac{\tilde{H}(t)}{\hbar} &= \omega_X(t)(a_X^\dagger a_X + 1/2) + \omega_Y(t)(a_Y^\dagger a_Y + 1/2) - \frac{\omega_Z}{2} \hat{\sigma}_Z \\ &+ i\sqrt{\frac{m^* \omega_X(t)}{2\hbar^3}} (a_X^\dagger - a_X) (\zeta_1(-\theta) \hat{\sigma}_X + \zeta_2(\theta) \hat{\sigma}_Z) + \frac{i}{4\omega_X(t)} \frac{\partial \omega_X(t)}{\partial t} \left((a_X^\dagger)^2 - a_X^2 \right) \\ &- i\sqrt{\frac{m^* \omega_Y(t)}{2\hbar^3}} (a_Y^\dagger - a_Y) (\zeta_2(-\theta) \hat{\sigma}_X + \zeta_1(-\theta) \hat{\sigma}_Z) + \frac{i}{4\omega_Y(t)} \frac{\partial \omega_Y(t)}{\partial t} \left((a_Y^\dagger)^2 - a_Y^2 \right) \\ &+ i \frac{\partial \omega_X(t)}{\partial t} \frac{eF_X}{\omega_X^2(t)} \sqrt{\frac{2}{\hbar m^* \omega_X(t)}} (a_X^\dagger - a_X) + i \frac{\partial \omega_Y(t)}{\partial t} \frac{eF_Y}{\omega_Y^2(t)} \sqrt{\frac{2}{\hbar m^* \omega_Y(t)}} (a_Y^\dagger - a_Y) \end{aligned} \quad (20)$$

$$\equiv \frac{1}{\hbar} \left(\tilde{H}_0(\omega_X, \omega_Y) + \sum_m \hat{V}_m \exp(im\omega_r t) \right) \quad (21)$$

where $a_{X(Y)}^\dagger$ and $a_{X(Y)}$ are the creation and annihilation operators associated with the harmonic potential, and $\omega_{X(Y)}(t) = \omega_{X(Y)} + \delta\omega_{X(Y)} \sin(\omega_r t + \phi_{X(Y)})$ is the time-dependent oscillator frequency. Note that $\tilde{H}_0(\omega_X, \omega_Y)$ contains the time-independent contributions to the energy from the harmonic potential and the Zeeman and spin-orbit interactions. In the presence of a static electric field (i.e., $F_{X(Y)} \neq 0$), modulations of ω_X and ω_Y also results in a modulation of \vec{r}_c , which leads to the terms linear in $a_{X(Y)}$ and $a_{X(Y)}^\dagger$ in Eq. (20).

Efficient transitions between the Floquet states $|1\rangle \equiv |0, 0, +, 1_F\rangle$ and $|2\rangle \equiv |0, 0, -, 0_F\rangle$ can be performed if the modulation frequency, ω_r , equals the energy difference between states $|1\rangle$ and $|2\rangle$, i.e., $\omega_r \approx \omega_Z$. Using Eq. (4), the effective Hamiltonian, $\hat{H}_{\text{EFF}}^{12}$, in the presence of parametric modulation of the oscillator strengths at $\omega_r \approx \omega_Z$ is given [up to $\delta\omega_{X(Y)}^2$]:

$$\hat{H}_{\text{EFF}}^{12} = \frac{\hbar}{2} (\omega_r - \omega_Z - \Delta_Z^{12} - \delta_Z) \hat{\sigma}_Z^{12} + \delta_+ \hat{\sigma}_+^{12} + \delta_- \hat{\sigma}_-^{12} \quad (22)$$

where $\hat{\sigma}_Z^{12} = |1\rangle\langle 1| - |2\rangle\langle 2|$, $\hat{\sigma}_+^{12} = |1\rangle\langle 2|$, $\hat{\sigma}_-^{12} = |2\rangle\langle 1|$, and

$$\begin{aligned} \Delta_Z^{12} &= \frac{m^* \omega_Z}{\hbar^3} \left(\frac{\omega_X (\zeta_1(-\theta))^2}{\omega_Z^2 - \omega_X^2} + \frac{\omega_Y (\zeta_2(-\theta))^2}{\omega_Z^2 - \omega_Y^2} \right) \\ \delta_Z &= \frac{m^* \omega_Z \delta\omega_X^2 (\zeta_1(-\theta))^2}{4\hbar^3 \omega_X} \left(\frac{32\omega_X^8 + 4\omega_X^6 \omega_Z^2 - 85\omega_X^4 \omega_Z^4 + 27\omega_X^2 \omega_Z^6 + 4\omega_Z^8}{(\omega_X^2 - 4\omega_Z^2)(4\omega_X^2 - \omega_Z^2)^2(\omega_X^2 - \omega_Z^2)^2} \right) \\ &+ \frac{m^* \omega_Z \delta\omega_Y^2 (\zeta_2(-\theta))^2}{4\hbar^3 \omega_Y} \left(\frac{32\omega_Y^8 + 4\omega_Y^6 \omega_Z^2 - 85\omega_Y^4 \omega_Z^4 + 27\omega_Y^2 \omega_Z^6 + 4\omega_Z^8}{(\omega_Y^2 - 4\omega_Z^2)(4\omega_Y^2 - \omega_Z^2)^2(\omega_Y^2 - \omega_Z^2)^2} \right) \\ &+ \frac{\omega_Z}{\hbar^4} \left((\delta\omega_X eF_X)^2 \frac{(\omega_X^2 + 3\omega_Z^2)(\zeta_1(-\theta))^2}{\omega_X^2 (\omega_Z^2 - \omega_X^2)^3} + (\delta\omega_Y eF_Y)^2 \frac{(\omega_Y^2 + 3\omega_Z^2)(\zeta_2(-\theta))^2}{\omega_Y^2 (\omega_Z^2 - \omega_Y^2)^3} \right) \\ &+ 2 \frac{eF_X eF_Y \delta\omega_X \delta\omega_Y}{\hbar^4} \cos(\phi_X - \phi_Y) \omega_Z \zeta_1(-\theta) \zeta_2(\theta) \frac{\omega_Z^2 (\omega_X^2 + \omega_Y^2) + \omega_X^2 \omega_Y^2 - 3\omega_Z^4}{\omega_X \omega_Y (\omega_X^2 - \omega_Z^2)^2 (\omega_Y^2 - \omega_Z^2)^2} \\ \delta_\pm &= -\frac{\omega_Z}{\hbar^2} \left(\frac{\zeta_1(-\theta) \delta\omega_X eF_X \exp(\pm i\phi_X)}{\omega_X (\omega_X^2 - \omega_Z^2)} - \frac{\zeta_2(-\theta) \delta\omega_Y eF_Y \exp(\pm i\phi_Y)}{\omega_Y (\omega_Y^2 - \omega_Z^2)} \right) \\ &\pm i \frac{m^* \omega_Z}{\hbar^3} \left(\exp(\pm i\phi_X) \frac{\zeta_1(-\theta) \zeta_2(\theta) \delta\omega_X}{4\omega_X^2 - \omega_Z^2} + \frac{\exp(\pm i\phi_Y) \zeta_1(\theta) \zeta_2(-\theta) \delta\omega_Y}{4\omega_Y^2 - \omega_Z^2} \right) \end{aligned} \quad (23)$$

where Δ_Z^{12} is the higher-order contribution of the spin-orbit coupling to the energy difference (in Eq. (23), Δ_Z^{12} is only written to second-order in the spin-orbit coupling), and δ_Z is a Bloch-Siegert shift³⁰ which arises from the noncommutivity of $\tilde{H}(t)$ at different times. In the presence of a static electric field, the coupling between the states $|1\rangle$ and $|2\rangle$, δ_\pm in Eq. (23), is first-order in the spin-orbit coupling parameters, whereas it is second-order in the spin-orbit coupling when $F_X = F_Y = 0$ eV/m.

Figure 2(A) presents the exact numerical simulation of the transition amplitude, $|\langle 0, 0, + | U(t, 0) | 0, 0, - \rangle|^2$, for a parabolic quantum dot under harmonic modulation of ω_X for $F_X \neq 0$. In the simulation, the eigenstates of $\tilde{H}_0(\omega_X, \omega_Y)$ in Eq. (20) were

numerically found by diagonalizing $\tilde{H}_0(\omega_X, \omega_Y)$ using a basis of four hundred $|n, m, \pm\rangle$ states. Next, $\tilde{H}(t)$ in Eq. (21) was expanded in the n lowest energy eigenstates of $\tilde{H}_0(\omega_X, \omega_Y)$, and $U(t) = T \exp(-i/\hbar \int_0^t \tilde{H}(t') dt')$ was then found numerically ($n = 30$ was found to give converged results for the simulations). The modulation frequency, ω_r , was given by the numerically calculated energy difference between the two states, ΔE_{12} , plus the Bloch- Siegert shift given in Eq. (23), i.e., $\omega_r = \Delta E_{12}/\hbar + \delta_Z \approx \omega_Z + \Delta_Z^2 + \delta_Z$. This method was used throughout the paper when numerically calculating the exact transition amplitudes.

The following parameters were used in the simulation shown in Fig. 2(A): $\hbar\omega_Y = \hbar\omega_X = 1$ meV, $\hbar\omega_Z = 0.1$ meV (corresponding to an in-plane magnetic field of around five Tesla in GaAs), $\alpha = 4 \times 10^{-13}$ eV-m, $m^* = 0.067m_0$ (where m_0 is the free electron mass), $\delta\omega_X = \omega_X/10$, $F_X = 10^4$ eV/m, and $\theta = 0$. With these parameters, the effective Rabi frequency for “on-resonance” modulation [$(\omega_r - \omega_Z)/(2\pi) = -3.46$ MHz] observed in Fig. 2(A) was 9.86 MHz, which is consistent with the theoretical value given by Eq. (23), $|\delta_{\pm}|/(2\pi) = 9.76$ MHz. The fact that the Rabi frequency is directly proportional to the spin-orbit coupling arises because modulation of ω_X results in a modulation of the effective center of the quantum dot \vec{r}_c by $\delta\vec{r}_c$ when $F_X \neq 0$. For the parameters used in Fig. 2(A), $|\delta\vec{r}_c| = 2.3$ nm.

For the case when $F_X = F_Y = 0$ eV/m, \vec{r}_c remains fixed, and the electron wave function is only squeezed/expanded during the modulation [Fig. 1(A)]. Figure 2(B) presents the exact numerical simulation of the transition amplitude, $|\langle 0, 0, +|U(t, 0)|0, 0, -\rangle|^2$, when $F_X = F_Y = 0$ eV/m. The following parameters were used: $\hbar\omega_Y = 1$ meV, $\hbar\omega_X = 0.25$ meV, $\hbar\omega_Z = 0.1$ meV, $\alpha = 8 \times 10^{-13}$ eV-m, $m^* = 0.067m_0$ (where m_0 is the free electron mass), $\delta\omega_X = \omega_X/20$, and $\theta = \pi/4$. With these parameters, the effective Rabi frequency observed in Fig. 2(B) was 355 kHz, which is consistent with the calculated value given by Eq. (23), $|\delta_{\pm}|/(2\pi) = 354$ kHz, for “on-resonance” irradiation, $(\omega_r - \omega_Z)/(2\pi) = -39.285$ MHz. The observed Rabi frequency was over an order of magnitude smaller than the case of nonzero F_X [Fig. 2(A)]. As stated earlier, the effective Rabi frequency is smaller since it is second-order in the spin-orbit coupling and contains terms like $(\alpha^2 - \beta^2)/2 \sin(2\theta) \pm \alpha\beta \cos(2\theta)$. Note that for $\theta = n\pi/2$, both α and β must be nonzero for δ_{\pm} to be nonzero. Furthermore, for the case when $\omega_X = \omega_Y$ and for uniform modulation (i.e. $\delta\omega_Y = \delta\omega_X$), the Rabi frequency in Eq. (23) is exactly proportional to $\alpha\beta \cos(2\theta)$. Finally, it should be noted that $\omega_r - \omega_Z$ is on the order of $|\delta_{\pm}|$ [Fig. 2(A)] or much greater than $|\delta_{\pm}|$ [Fig. 2(B)], so that ω_r must be tuned with precision given by $|\delta_{\pm}|$ in order to maximize the amplitude of the Rabi oscillations.

Although Eq. (4) was used to generate $\hat{H}_{\text{EFF}}^{12}$ in Eqs. (22)-(23), the dynamics under modulations of ω_X and ω_Y can be calculated using the following time-dependent Hamiltonian:

$$\hat{H}(t) = \frac{\hat{P}_X^2}{2m^*} + \frac{\hat{P}_Y^2}{2m^*} + \hat{H}_{SO} - \frac{\hbar\omega_Z}{2}\hat{\sigma}_Z + \frac{m^*}{2} \left(\omega_X^2(t)\hat{X}^2 + \omega_Y^2(t)\hat{Y}^2 \right) - eF_X\hat{X} - eF_Y\hat{Y} \quad (24)$$

where $\hat{P}_{X(Y)} = \sqrt{m^*\hbar\omega_{X(Y)}/2i}(a_{X(Y)}^\dagger - a_{X(Y)})$, $\hat{X}(\hat{Y}) = \sqrt{\hbar/(2m^*\omega_{X(Y)})} (a_{X(Y)} + a_{X(Y)}^\dagger)$, and $\omega_{X(Y)}(t) = \omega_{X(Y)} + \delta\omega_{X(Y)}(t)$. $\hat{H}(t)$ in Eq. (24) can be used to construct an effective Hamiltonian in the $|0, 0, +, 1_F\rangle$ and $|0, 0, -, 0_F\rangle$ subspace, which is also given by Eqs. (22)-(23).

B. Parametric Modulations of a Parabolic Quantum Dot's center

In addition to modulating the confinement frequency, the center of the parabolic quantum dot can also be modulated, i.e. $x_c \rightarrow x_c + \delta x_c(t)$ and $y_c \rightarrow y_c + \delta y_c(t)$. Unlike the case of modulating ω_X and ω_Y , displacements of the harmonic potential do not alter the energy spacings of the quantum dot; however, the simultaneous eigenstates of the oscillator do change under such modulation. Using Eq. (4), the Hamiltonian under time-dependent displacements of the parabolic potential's center is given by:

$$\begin{aligned} \frac{\tilde{H}(t)}{\hbar} &= \omega_X(a_X^\dagger a_X + 1/2) + \omega_Y(a_Y^\dagger a_Y + 1/2) - \frac{\omega_Z}{2}\hat{\sigma}_Z \\ &+ i\sqrt{\frac{m^*\omega_X}{2\hbar^3}} (a_X^\dagger - a_X) (\zeta_1(-\theta)\hat{\sigma}_X + \zeta_2(\theta)\hat{\sigma}_Z) - i\sqrt{\frac{m^*\omega_X}{2\hbar}} \frac{\partial x_c(t)}{\partial t} (a_X^\dagger - a_X) \\ &- i\sqrt{\frac{m^*\omega_Y}{2\hbar^3}} (a_Y^\dagger - a_Y) (\zeta_1(\theta)\hat{\sigma}_Z + \zeta_2(-\theta)\hat{\sigma}_X) - i\sqrt{\frac{m^*\omega_Y}{2\hbar}} \frac{\partial y_c(t)}{\partial t} ((a_Y^\dagger) - a_Y) \end{aligned} \quad (25)$$

For small displacements, $x_c \rightarrow x_c + \delta x_c \sin(\omega_r t + \phi_X)$ and $y_c \rightarrow y_c + \delta y_c \sin(\omega_r t + \phi_Y)$, the effective Hamiltonian in the $|0, 0, +, 1_F\rangle$ and $|0, 0, -, 0_F\rangle$ subspace can be written as (for $\omega_r \approx \omega_Z$):

$$\frac{\hat{H}_{\text{EFF}}^{12}}{\hbar} = \frac{1}{2} (\omega_r - \omega_Z + \delta_Z^c + \Delta_Z^{12}) \hat{\sigma}_Z^{12} + \delta_+^c \hat{\sigma}_+^{12} + \delta_-^c \hat{\sigma}_-^{12} \quad (26)$$

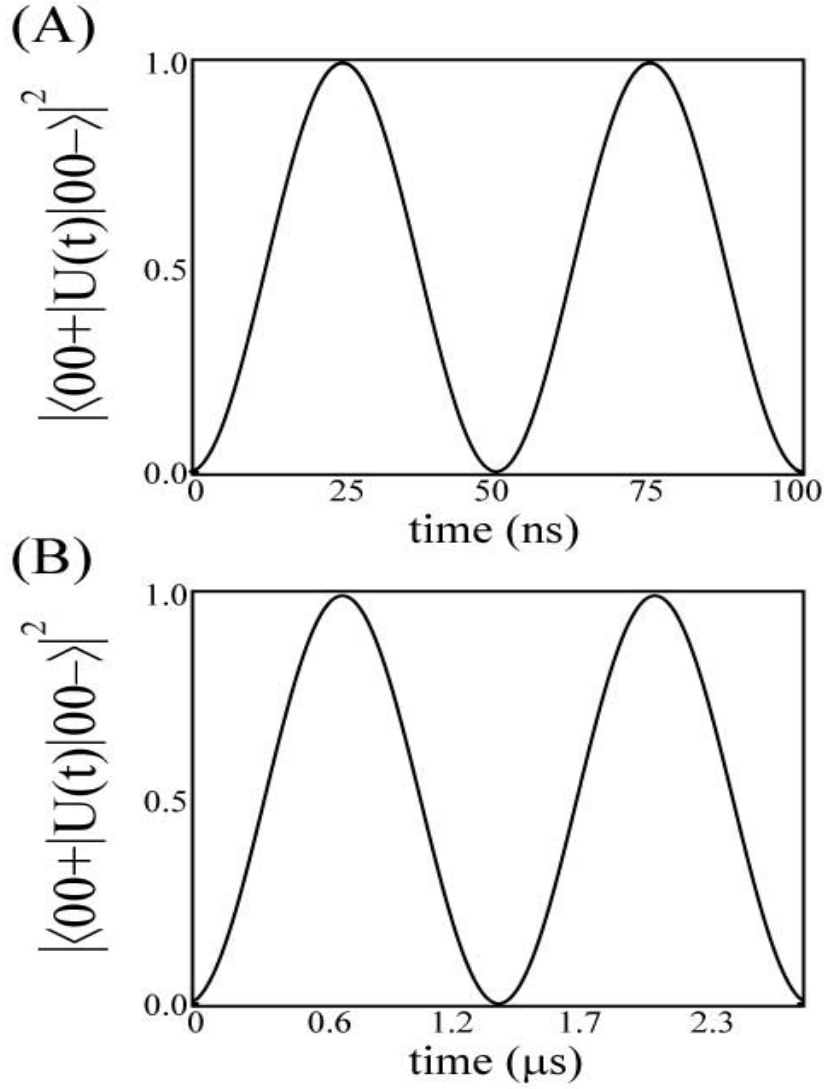


FIG. 2: Numerical simulation of the transition amplitudes, $|\langle 0, 0, +|T \exp(-i \int_0^t dt' \tilde{H}(t'))|0, 0, -\rangle|^2$, caused by modulating a quantum dot's oscillator frequency, $\omega_X(t) = \omega_X + \delta\omega_X \sin(\omega_r t)$, (A) with and (B) without a static electric field. In the presence of a static electric field, the effective Rabi frequency is first-order in the spin-orbit coupling [Eq. (23)], which lead to a large Rabi frequency as shown in Fig. 2(A). The following parameters were used in the simulation: $\hbar\omega_Y = \hbar\omega_X = 1$ meV, $\alpha = 4 \times 10^{-13}$ eV-m, $\beta = 0$ eV-m, $\hbar\omega_Z = 0.1$ meV, $\theta = 0$, $\delta\omega_X = \frac{\omega_X}{10}$, $F_X = 10^4$ eV/m, and $\phi_X = 0$, which gave a Rabi frequency of 9.86 MHz compared with the calculated value of $|\delta_{\pm}|/(2\pi) \approx 9.77$ MHz by Eq. (23). In the absence of a static electric field, the effective Rabi frequency is second-order in the spin-orbit coupling, which lead to a smaller Rabi frequency as shown in Fig. 2(B). The following parameters were used: $\hbar\omega_Y = 1$ meV, $\hbar\omega_X = 0.25$ meV, $\hbar\omega_Z = 0.1$ meV, $\alpha = 8 \times 10^{-13}$ eV-m, $\delta\omega_X = \omega_X/20$, $\beta = 0$ eV-m, $\theta = \pi/4$, $F_X = 0$ eV/m, and $\phi_X = 0$, which gave a Rabi frequency of 355 kHz compared with the calculated value of $|\delta_{\pm}|/(2\pi) = 354$ kHz given by Eq. (23).

where

$$\delta_Z^c = \frac{(m^*)^2 \omega_Z}{4\hbar^4} \left((\delta x_c)^2 \frac{\omega_X^4 (\omega_X^2 + 3\omega_Z^2) (\zeta_1(-\theta))^2}{(\omega_Z^2 - \omega_X^2)^3} + (\delta y_c)^2 \frac{\omega_Y^4 (\omega_Y^2 + 3\omega_Z^2) (\zeta_2(-\theta))^2}{(\omega_Z^2 - \omega_Y^2)^3} \right) + \frac{(m^* \omega_X \omega_Y)^2}{2\hbar^4} \cos(\phi_X^c - \phi_Y^c) \delta y_c \delta x_c \omega_Z \zeta_1(-\theta) \zeta_2(\theta) \frac{\omega_Z^2 (\omega_X^2 + \omega_Y^2) + \omega_X^2 \omega_Y^2 - 3\omega_Z^4}{(\omega_X^2 - \omega_Z^2)^2 (\omega_Y^2 - \omega_Z^2)^2} \quad (27)$$

$$\delta_{\pm}^c = -\frac{m^* \omega_Z}{2\hbar^2} \left(\exp(\pm i \phi_X^c) \delta x_c \frac{\omega_X^2 \zeta_1(-\theta)}{\omega_Z^2 - \omega_X^2} - \exp(\pm i \phi_Y^c) \delta y_c \frac{\omega_Y^2 \zeta_2(-\theta)}{\omega_Z^2 - \omega_Y^2} \right) \quad (28)$$

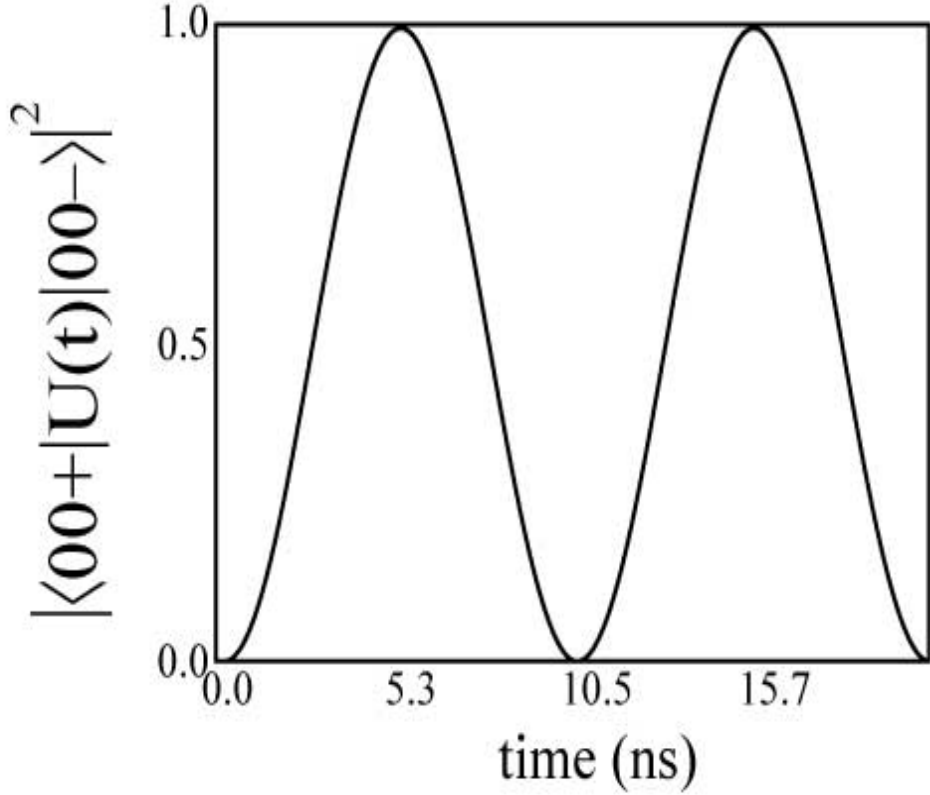


FIG. 3: Numerical simulation of the transition amplitudes, $|\langle 0, 0, + | T \exp(-i \int_0^t dt' \tilde{H}(t')) | 0, 0, - \rangle|^2$, caused by modulating the center of the quantum dot's parabolic potential. In this case, the effective Rabi frequency is first-order in the spin-orbit coupling [Eq. (28)], leading to a large Rabi frequency. The following parameters were used in the simulation: $\hbar\omega_Y = \hbar\omega_X = 1$ meV, $\alpha = 4 \times 10^{-13}$ eV-m, $\beta = 0$ eV-m, $\hbar\omega_Z = 0.1$ meV, $\theta = 0$, $\delta x_c = 11.5$ nm [equivalent to using an electric field of $E_X = 10^4$ eV/m], and $\phi_X = 0$, which gave a Rabi frequency of 48.7 MHz compared with calculated value of $|\delta_{\pm}^{\text{EF}}|/(2\pi) \approx 48.8$ MHz given by Eq. (28).

The effective coupling between spin states, δ_{\pm}^c , is first-order in the spin-orbit coupling, which leads to large Rabi frequencies. Figure 3 presents an exact numerical simulation of the transition amplitude, $|\langle 0, 0, + | T \exp(-i \int_0^t dt' \tilde{H}(t')/\hbar) | 0, 0, - \rangle|^2$, in the presence of modulating the center of the parabolic well. The following parameters were used in the simulation: $\hbar\omega_X = \hbar\omega_Y = 1$ meV, $\alpha = 4 \times 10^{-13}$ eV-m, $\beta = 0$ eV-m, $\hbar\omega_Z = 0.1$ meV, $\theta = 0$, $F_X = F_Y = 0$ eV/m, and $\delta x_c = 11.4$ nm. Such parameters gave an effective Rabi frequency of 48.7 MHz in Fig. 3 compared with the calculated value of $|\delta_{\pm}^c|/(2\pi) = 48.8$ MHz given by Eq. (28) for “on-resonance” modulation (i.e., $(\omega_r - \omega_Z)/(2\pi) = -3.435$ MHz). As mentioned in the introduction, parametric modulation of a parabolic quantum dot's center is equivalent to applying a time-dependent electric field, $E(t) = E_X(t)\hat{x} + E_Y(t)\hat{y}$, with the correspondence that $\delta x_c(t) = eE_X(t)/(m^*\omega_X^2)$ and $\delta y_c(t) = eE_Y(t)/(m^*\omega_Y^2)$. The simulation in Fig. 3 corresponds to $E_X = 10^4$ eV/m. Previous theoretical work has suggested using such EDSR methods to perform efficient spin rotations in quantum wells^{8,9,10} and quantum dots^{11,12}.

C. Determining the spin-orbit coupling constants, α and β

In the above examples of parametric oscillations, both the effective Rabi frequency, δ_{\pm} , and the effective offset, Δ_Z , depend upon the spin-orbit coupling constants of the quantum dot (α and β), the oscillator frequencies (ω_X and ω_Y), and the direction of the magnetic field, θ . This dependence can potentially be used to determine both the spin-orbit coupling constants α and β . For instance, consider the effects of modulating the center of the parabolic dot, i.e., performing an EDSR experiment. Taking the ratio of the “measured” Rabi frequency [Eq. (28)] for an experiment with $\delta x_c = \lambda_{\text{mod}}$ and $\delta y_c = 0$ to the “measured” Rabi

frequency for an experiment with $\delta x_c = 0$ and $\delta y_c = \lambda_{\text{mod}}$ gives

$$\begin{aligned} ZZ(\theta) &= \frac{\delta_{\pm}(\delta x_c = \lambda_{\text{mod}}, \delta y_c = 0), \theta}{\delta_{\pm}(\delta x_c = 0, \delta y_c = \lambda_{\text{mod}}, \theta)} \\ &= -\frac{\zeta_1(-\theta)}{\zeta_2(-\theta)} \end{aligned} \quad (29)$$

For an in-plane magnetic field along the \hat{y} axis (i.e., $\theta = \pi/2$), the relative ratio of the spin-orbit coupling strengths can be found since in this case $ZZ(\pi/2) = \beta/\alpha$. Furthermore, Δ_Z , which can be determined by tuning ω_r to the frequency which maximizes the amplitude of the Rabi oscillations and then approximating $\Delta_Z \approx \omega_r - \omega_Z$, can then be used to determine the absolute value of α and β . Although the calculations used in this section were for a harmonic potential, more realistic $\hat{V}(\hat{X}, \hat{Y})$ using the full electrostatic potential generated by the metallic surface gates³¹ could be used to more accurately characterize the spin dynamics in terms of α and β under parametric modulation of $\hat{V}(\hat{X}, \hat{Y})$.

IV. THE EFFECTS OF THE CUBIC DRESSELHAUS SPIN-ORBIT INTERACTION

Recent work has indicated that the cubic Dresselhaus term can become the dominant spin-orbit interaction in highly confined (i.e., large ω_X and ω_Y) quantum dots³². For the coordinate system chosen in this work, the cubic Dresselhaus term is given by:

$$\hat{H}_D^{\text{cub}} = \frac{\gamma}{\hbar^3} \left(\hat{P}_Y \hat{P}_X \hat{P}_Y (\cos(\theta) \hat{\sigma}_Z - \sin(\theta) \hat{\sigma}_X) - \hat{P}_X \hat{P}_Y \hat{P}_X (\sin(\theta) \hat{\sigma}_Z + \cos(\theta) \hat{\sigma}_X) \right) \quad (30)$$

The linear Dresselhaus coupling, β in Eq. (18), is related to the cubic Dresselhaus coupling constant, γ in Eq. (30), by $\beta = \gamma \langle \hat{P}_Z^2 \rangle / \hbar^2$ [where for a quantum well of width l_w , $\langle \hat{P}_Z^2 \rangle / \hbar^2 \approx (\pi/l_w)^2$]. For a quantum well with $l_w = 30$ nm, and for $\hbar\omega_{X(Y)} \approx 1$ meV, the relative strength of the cubic and linear Dresselhaus terms is given roughly by $\langle \hat{P}_{X(Y)}^2 \rangle / \langle \hat{P}_Z^2 \rangle \approx m^* \omega_{X(Y)} l_w^2 / (2\pi^2 \hbar) = 0.04$. The larger ω_X and ω_Y are for the quantum dot, the more the cubic Dresselhaus coupling contributes to the total spin-orbit interaction.

Under parametric modulation of the center of the quantum dot (i.e., an EDSR experiment), the effect of the cubic Dresselhaus coupling can be found by simply adding \hat{H}_D^{cub} to $\tilde{H}(t)$ in Eq. (25). The effective Hamiltonian in the $|1\rangle = |0, 0, +, 1_F\rangle$ and $|2\rangle = |0, 0, -, 0_F\rangle$ subspace in this case is given by:

$$\frac{\hat{H}_{\text{cub}}^{12}}{\hbar} = \frac{1}{2} (\omega_r - \omega_Z - \Delta_{Z,\text{cub}}^{12}) \hat{\sigma}_Z^{12} + \delta_{+,\text{cub}}^c \hat{\sigma}_+^{12} + \delta_{-,\text{cub}}^c \hat{\sigma}_-^{12} \quad (31)$$

where

$$\begin{aligned} \Delta_{Z,\text{cub}}^{12} &= \frac{m^* \omega_Z}{\hbar^3} \left(\frac{\omega_X (\zeta_1^{\text{cub}}(-\theta))^2}{\omega_Z^2 - \omega_X^2} + \frac{\omega_Y (\zeta_2^{\text{cub}}(-\theta))^2}{\omega_Z^2 - \omega_Y^2} \right) \\ &\quad - \frac{m^* \omega_Z}{2\hbar} \left(\frac{m^* \gamma}{\hbar^2} \right)^2 \omega_X \omega_Y \left(\frac{\omega_Y \sin^2(\theta)}{(2\omega_Y + \omega_X)^2 - \omega_Z^2} + \frac{\omega_X \cos^2(\theta)}{(2\omega_X + \omega_Y)^2 - \omega_Z^2} \right) \\ \delta_{\pm,\text{cub}}^c &= -\frac{m^* \omega_Z}{2\hbar^2} \left(\frac{\exp(\pm i\phi_X^c) \delta x_c \omega_X^2 \zeta_1^{\text{cub}}(-\theta)}{\omega_Z^2 - \omega_X^2} - \frac{\exp(\pm i\phi_Y^c) \delta y_c \omega_Y^2 \zeta_2^{\text{cub}}(-\theta)}{\omega_Z^2 - \omega_Y^2} \right) \end{aligned} \quad (32)$$

with $\zeta_1^{\text{cub}}(-\theta) = \alpha \cos(\theta) + [\beta - \gamma m^* \omega_Y / (2\hbar)] \sin(\theta)$ and $\zeta_2^{\text{cub}}(-\theta) = -(\alpha \sin(\theta) + [\beta - \gamma m^* \omega_X / (2\hbar)] \cos(\theta))$. Since γ and β have the same sign, the cubic Dresselhaus interaction lessens the contribution of the linear Dresselhaus interaction to the effective Rabi frequency under parametric modulation of the electrostatic potential. Similar results are also obtained in the case of modulating ω_X and ω_Y ; in this case, the effective Rabi frequency is again proportional to the spin-orbit coupling parameters only in the presence of a nonzero static electric field, $F_{X(Y)} \neq 0$ [otherwise, it is second-order in the spin-orbit coupling parameters].

Under parametric modulation of both the quantum dot's center and oscillator frequency, Rabi oscillations, which depend only upon γ , can occur; measuring the Rabi frequency^{15,16} would therefore provide an independent measurement of γ . Consider the case when the quantum dot's center is modulated about the \hat{y} direction at a frequency of ω_{r1} , $y_c(t) = \delta y_c \sin(\omega_{r1}t + \phi_Y)$, while at the same time the quantum dot is being periodically squeezed about the \hat{x} direction at a frequency of ω_{r2} , $\omega_X(t) = \omega_X + \delta\omega_X \sin(\omega_{r2}t + \phi_X)$. In this case, efficient spin rotations can be performed in the relevant bimodal Floquet subspace, $|1\rangle = |0, 0, +, 1_{F1}, 1_{F2}\rangle$ and $|2\rangle = |0, 0, -, 0_{F1}, 0_{F2}\rangle$ when $\omega_{r1} + \omega_{r2} \approx \omega_Z$ [here F_1 and F_2 denote the Floquet states relative to the oscillator frequencies ω_{r1} and ω_{r2} respectively]. The effective Hamiltonian in this subspace can be written as:

$$\frac{\hat{H}_{\text{cub}}^{12}}{\hbar} = \frac{1}{2} (\omega_{r1} + \omega_{r2} - \omega_Z - \Delta_{Z,\text{cub}}^{12} - \delta_{Z,\text{cub}}^{12}) \hat{\sigma}_Z^{12} + \delta_{+,\text{cub}}^{12} \hat{\sigma}_+^{12} + \delta_{-,\text{cub}}^{12} \hat{\sigma}_-^{12} \quad (33)$$

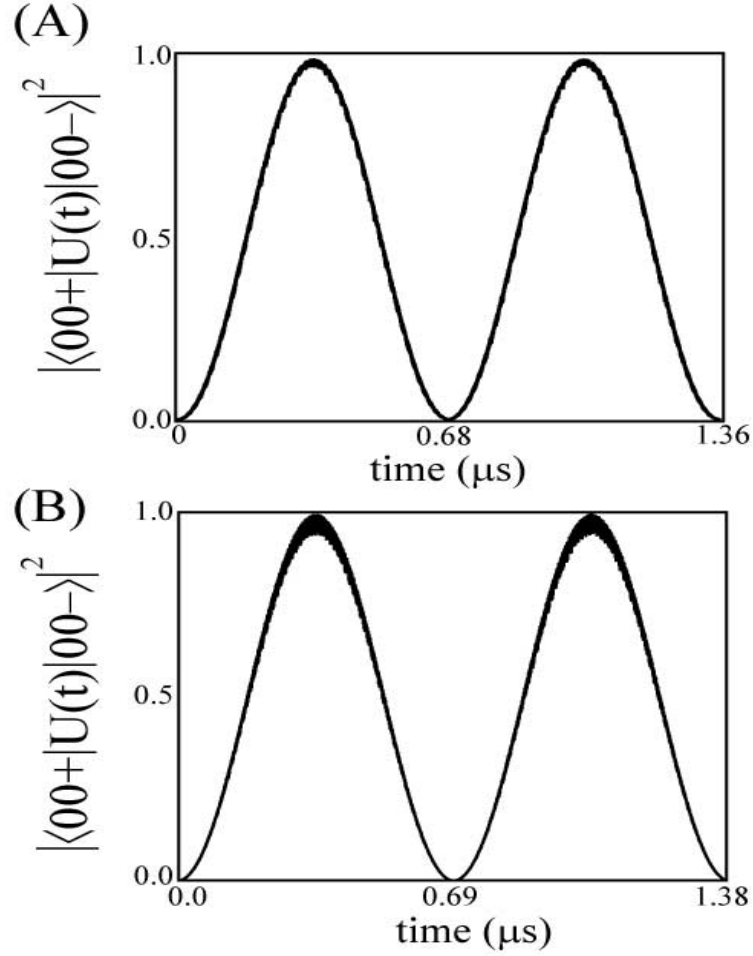


FIG. 4: Numerical simulation of the transition amplitudes, $|\langle 0, 0, + | T \exp(-i \int_0^t dt' \tilde{H}(t')) | 0, 0, - \rangle|^2$, caused by the simultaneous modulation of the quantum dot's oscillator frequency $[\omega_X(t) = \omega_X + \delta\omega_X \sin(\omega_{r2}t)]$ and center $[y_c(t) = \delta y_c \sin(\omega_{r1}t)]$, (A) with and (B) without the Rashba and linear Dresselhaus spin-orbit interaction. Efficient spin transitions, which depend upon the cubic Dresselhaus coupling to first-order, can be performed when $\omega_{r1} + \omega_{r2} \approx \omega_Z$ [Eq. (35)]. In both simulations, the following parameters were used: $\hbar\omega_Y = 0.45$ meV, $\hbar\omega_X = 3$ meV, $\hbar\omega_Z = 0.1$ meV, $\theta = 0$, $\delta\omega_X = \frac{\omega_X}{10}$, $\omega_{r1} = 2\omega_{r2}$, $\delta y_c = 56$ nm (equivalent to $E_Y = 10^4$ eV/m), $\gamma = 27 \times 10^{-30}$ eV-m³, and $\phi_X = \phi_Y = 0$. In (A), $\alpha = 4 \times 10^{-13}$ eV-m and $l_w = 30$ nm (giving $\beta = 2.96 \times 10^{-13}$ eV-m), which gave a sizable Bloch-Siegert shift of $\delta_{Z,\text{cub}}^{12}/(2\pi) = 3.32$ MHz. In Fig. 4(A), the observed Rabi frequency was 736.6 kHz, which is within 2% of the calculated theoretical value given by Eq. (35), $|\delta_{\pm,\text{cub}}^{12}|/(2\pi) = 721.5$ kHz. In (B), the linear Dresselhaus and Rashba spin-orbit coupling constants were artificially set to zero, resulting in $\delta_{Z,\text{cub}}^{12}/(2\pi) \approx 400$ kHz; the observed Rabi frequency was 724.5 kHz, which is similar to that observed in Fig. 4(A) and is closer to the calculated value given by Eq. (35). This demonstrates that the observed Rabi oscillations are mainly due to the cubic Dresselhaus coupling [differences between (A) and (B) are mainly due to higher-order coupling terms involving α and β].

where

$$\delta_{Z,\text{cub}}^{12} \approx \left(\frac{m^* \delta y_c}{\hbar^2} \right)^2 \frac{\omega_{r1}^2 \omega_Y^4 \omega_Z (\zeta_2^{\text{cub}}(-\theta))^2}{(\omega_{r1}^2 - \omega_Y^2)^2 (\omega_Z^2 - \omega_{r1}^2)} \quad (34)$$

$$\delta_{\pm,\text{cub}}^{12} = \pm \frac{i\gamma \cos(\theta)}{2\hbar^3} \exp(\pm i(\phi_X + \phi_Y)) \frac{\delta\omega_X \delta y_c \omega_{r1} (m^* \omega_X \omega_Y)^2}{(\omega_{r1}^2 - \omega_Y^2)(\omega_{r2}^2 - 4\omega_X^2)} \quad (35)$$

The effect of the linear Dresselhaus and Rashba spin-orbit coupling arises mainly in the Bloch-Siegert shift, $\delta_{Z,\text{cub}}^{12}$, and in $\Delta_{Z,\text{cub}}^{12}$; higher-order terms contributions to $\delta_{\pm,\text{cub}}^{12}$ arising from both the linear Dresselhaus and Rashba spin-orbit coupling can be made negligible by using smaller $\delta\omega_X$ and δy_c .

Figure 4 shows the numerical simulation of $|\langle 0, 0, + | T \exp(-\frac{i}{\hbar} \int_0^t \tilde{H}(t') dt') | 0, 0, - \rangle|^2$ under both periodic modulation of the quantum dot's center about the \hat{y} direction and modulation of the oscillator frequency about the \hat{x} direction in (A) the presence of

and in (B) the absence of the Rashba and linear Dresselhaus spin-orbit interactions. In Fig. 4(A), the following parameters were used: $\hbar\omega_X = 3$ meV, $\hbar\omega_Y = 0.45$ meV, $\hbar\omega_Z = 0.1$ meV, $\delta\omega_X = \omega_X/10$, $\omega_{r1} = 2\omega_{r2}$, $\gamma = 27 \times 10^{-30}$ eV-m³, $\alpha = 4 \times 10^{-13}$ eV-m, $l_w = 30$ nm (giving $\beta \approx 2.96 \times 10^{-13}$ eV-m), and $\delta y_c = 56$ nm (giving $E_Y \approx 10^4$ eV/m). With the above parameters, $\delta_{Z,\text{cub}}^{12}/(2\pi) \approx 3.33$ MHz. The observed Rabi frequency in Fig. 4(A) was 736.6 kHz, which is within 2% of the calculated value given by Eq. (35), $|\delta_{\pm,\text{cub}}^{12}|/(2\pi) = 721.5$ kHz. Since $\delta_{Z,\text{cub}}^{12} > |\delta_{\pm,\text{cub}}^{12}|$, ω_{r1} and ω_{r2} must be tuned to include $\delta_{Z,\text{cub}}^{12}$ in order to maximize the amplitude of the Rabi oscillations [in Fig. 4(A), $(\omega_{r1} + \omega_{r2} - \omega_Z)/(2\pi) = -4.504$ MHz + $\delta_{Z,\text{cub}}^{12}/(2\pi)$]. Note also that in the numerical simulation of Fig. 4(A), the transition amplitude does not go exactly to 1 (maximum value of 0.9861), which is most likely due to higher-order corrections to the Bloch-Siegert shift, $\delta_{Z,\text{cub}}^{12}$.

Better agreement between the Rabi frequency calculated using Eq. (35) to numerical simulation is obtained in Fig. 4(B) where both α and β were artificially set to zero, removing the dominant higher-order corrections to both $\delta_{Z,\text{cub}}^{12}$ and $\delta_{\pm,\text{cub}}^{12}$. In Fig. 4(B), the observed Rabi frequency was 724.5 kHz, which is closer to the calculated value given by Eq. (35), $|\delta_{\pm,\text{cub}}^{12}|/(2\pi) = 721.5$ kHz. It should be noted that both simulations shown in Fig. 4 give roughly the same Rabi frequency, which, to a good approximation, is given by Eq. (35). Thus measuring the Rabi frequency under such parametric modulations should enable γ to be directly determined. It should be noted that for a quantum dot with a non-harmonic potential and in the presence of an out of plane magnetic field, it has previously¹¹ been found that the EDSR technique also generates spin rotations which, to first order, depend upon γ and the cyclotron frequency.

V. PARAMETRIC MODULATIONS IN SQUARE QUANTUM DOTS

Besides harmonic potentials, another model electrostatic potential for electrons in lateral quantum dots is that of a square-box (hard wall) potential defined by $V(x, y) = 0$ for $0 \leq x \leq L_X$ and $0 \leq y \leq L_Y$ and $V(x, y) = \infty$ everywhere else. Although the hard wall potential is not very realistic in two-dimensional systems, previous studies have utilized such models in analyzing transport in quantum dots^{33,34}, and such potentials are the quintessential model for studies of chaos in two-dimensional systems, such as in the stadium billiard^{35,36}. For the square-box potential, the eigenstates for \hat{H}_0 are simply the two-dimensional particle in a box states, $\langle \vec{r} | n, m, \pm \rangle = \sqrt{\frac{2}{L_X}} \sqrt{\frac{2}{L_Y}} \sin\left(\frac{\pi n x}{L_X}\right) \sin\left(\frac{\pi m y}{L_Y}\right) | \pm \rangle$. In order to induce transitions between the various $|n, m, \pm\rangle$, small, periodic modulations in both the length and the width of the box, L_X and L_Y , can be made. Using Eq. (4), the effective time-dependent Hamiltonian during modulation of the box's length and width, $L_X \rightarrow L_X(t)$ and $L_Y \rightarrow L_Y(t)$, can be written as:

$$\begin{aligned} \frac{\tilde{H}(t)}{\hbar} &= \frac{\hbar\pi^2}{2m^*L_X^2(t)}\hat{H}_X + \frac{\hbar\pi^2}{2m^*L_Y^2(t)}\hat{H}_Y - \frac{\omega_Z}{2}\hat{\sigma}_Z \\ &+ \frac{L_X}{\hbar^2L_X(t)}\hat{P}_X(\zeta_1(-\theta)\sigma_X + \zeta_2(\theta)\hat{\sigma}_Z) - \frac{L_Y}{\hbar L_Y(t)}\hat{P}_Y(\zeta_1(\theta)\sigma_Z + \zeta_2(-\theta)\hat{\sigma}_X) \\ &+ \frac{\partial L_X(t)}{\partial t} \frac{1}{2\hbar L_X(t)} \left(\hat{P}_X \hat{X} + \hat{X} \hat{P}_X \right) + \frac{\partial L_Y(t)}{\partial t} \frac{1}{2\hbar L_Y(t)} \left(\hat{P}_Y \hat{Y} + \hat{Y} \hat{P}_Y \right) \end{aligned} \quad (36)$$

where

$$\begin{aligned} \hat{H}_X &= \sum_{n,m,\pm} n^2 |n, m, \pm\rangle \langle n, m, \pm| \\ \hat{H}_Y &= \sum_{n,m,\pm} m^2 |n, m, \pm\rangle \langle n, m, \pm| \end{aligned} \quad (37)$$

The form of $\tilde{H}(t)$ arises naturally from Eq. (4); previous work on parametric deformations of hard wall potentials have also arrived at a similar form for the effective Hamiltonian^{37,38}. Note, however, that it is necessary to separate the transformation $\hat{W}(t)$ from the dynamics and only include its effect at the end of the calculation³⁹.

By performing small modulations of the length and width, $L_X \rightarrow L_X + \delta L_X(t)$ and $L_Y \rightarrow L_Y + \delta L_Y(t)$, spin transitions can be performed due to the spin-orbit interaction. The effective Hamiltonian in the $|1\rangle \equiv |1, 1, +, 1_F\rangle$ and $|2\rangle \equiv |1, 1, -, 0_F\rangle$ Floquet subspace is given to first-order in $\delta L_{X(Y)}(t)$ and for $\omega_r \approx \omega_Z$ as:

$$\frac{\hat{H}_{\text{EFF}}^{12}}{\hbar} = \frac{1}{2} (\omega_r - \omega_Z + \Delta_Z^{12}) \hat{\sigma}_Z^{12} + \delta_+ \hat{\sigma}_+^{12} + \delta_- \hat{\sigma}_-^{12} \quad (38)$$

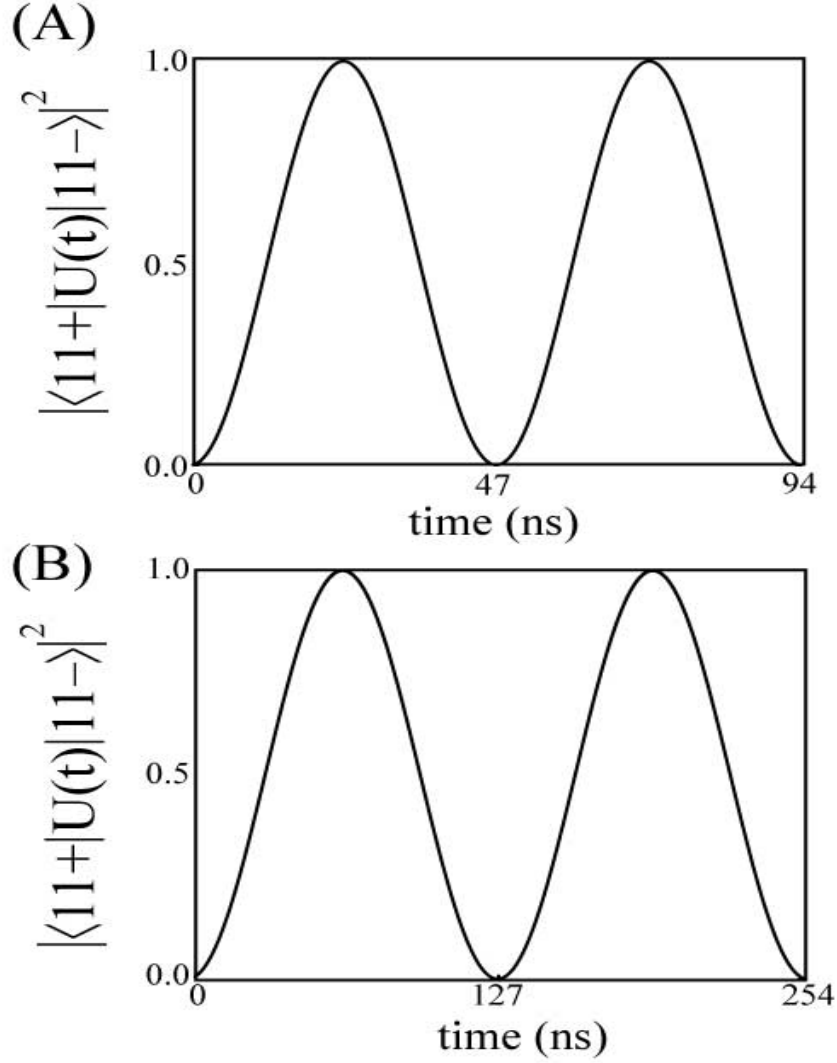


FIG. 5: Numerical simulation of the transition amplitudes, $|\langle 1, 1, + | T \exp(-i \int_0^t dt' \tilde{H}(t')) | 1, 1, - \rangle|^2$, in a square quantum dot caused by either (A) modulating the size of the quantum dot or (B) by applying a time-dependent electric field. In both cases, the Rabi frequency is first-order in the spin-orbit coupling strength. The parameters used in both simulations were $L_X = L_Y = 70$ nm [giving $\hbar^2 \pi^2 / (2m^* L_{X(Y)}^2) = 1.1$ meV], $\alpha = 4 \times 10^{-13}$ eV-m, $\beta = 0$ eV-m, $\hbar\omega_Z = 0.1$ meV, $\theta = 0$, $(\omega_r - \omega_Z)/(2\pi) = -958.4$ kHz, and $\phi_X = 0$. In (A), $L_X(t) = L_X + \delta L_X \sin(\omega_r t)$ with $\delta L_X = 5$ nm, which gave an effective Rabi frequency of 10.6 MHz, which is in excellent agreement with the calculated value given by Eq. (40), $|\delta_{\pm}|/(2\pi) = 10.6$ MHz. In (B), the applied electric field was $\vec{E}(t) = E_X \sin(\omega_r t) \hat{x}$ with $E_X = 10^4$ eV/m, which gave an effective Rabi frequency of 3.94 MHz, which is in excellent agreement with the calculated value given by Eq. (42), $|\delta_{\pm}^{\text{EF}}|/(2\pi) = 3.92$ MHz.

where

$$\Delta_Z^{12} = \frac{32m^*}{\pi^2 \hbar^3} \sum_{n=2}^{\infty} \frac{n^2 (1 + (-1)^n)}{(n^2 - 1)^2} \left(\frac{(\zeta_1(-\theta))^2 \eta_X}{(n^2 - 1)^2 - (\eta_X)^2} + \frac{(\zeta_2(-\theta))^2 \eta_Y}{(n^2 - 1)^2 - (\eta_Y)^2} \right) \quad (39)$$

$$\delta_{\pm} = \frac{4}{\hbar} \sum_{n=2}^{\infty} \frac{n^2 (1 + (-1)^n)}{1 - n^2} \left(\frac{\zeta_1(-\theta) \eta_X \delta L_X \exp(\pm i \phi_X)}{L_X^2 ((n^2 - 1)^2 - \eta_X^2)} - \frac{\zeta_2(-\theta) \eta_Y \delta L_Y \exp(\pm i \phi_Y)}{L_Y^2 ((n^2 - 1)^2 - \eta_Y^2)} \right) \quad (40)$$

where $\eta_{X(Y)} = 2m^* \omega_Z L_{X(Y)}^2 / (\hbar \pi^2)$. By choosing $\omega_r = \omega_Z - \Delta_Z^{12}$, efficient spin transitions can be generated in square quantum dots [Fig. 5(A)] since the Rabi frequency, $|\delta_{\pm}|/(2\pi)$, is directly proportional to the spin-orbit coupling strength, in contrast

to a parabolic quantum dot undergoing modulations of confining frequency and in the absence of a static electric field [Eq. (23)]. Figure 5(A) presents an exact numerical simulation of the transition amplitude, $|\langle 1, 1, + | T \exp(-i \int_0^t dt' \tilde{H}(t')/\hbar) | 1, 1, - \rangle|^2$, in the presence of modulating the effective size of a square quantum dot. The following parameters were used in the simulation: $L_X = L_Y = 70$ nm [giving $\hbar^2 \pi^2 / (2m^* L_{X(Y)}^2) \approx 1.1$ meV and $\eta_{X(Y)} = 0.087$], $\delta L_X = 5$ nm, $\alpha = 4 \times 10^{-13}$ eV-m, $\beta = 0$ eV-m, $\hbar \omega_Z = 0.1$ meV, $\theta = 0$, and $(\omega_r - \omega_Z)/(2\pi) = -958.4$ kHz. Such parameters gave an effective Rabi frequency of 10.6 MHz, which is in excellent agreement with the calculated value given by Eq. (40), $|\delta_+|/(2\pi) = 10.6$ MHz.

Alternatively, an electric field, $\vec{E}(t) = E_X \sin(\omega_r t + \phi_X) \hat{x} + E_Y \sin(\omega_r t + \phi_Y) \hat{y}$, applied to the quantum dot can also induce single spin rotations by using EDSR effects. Incorporating the interaction with the electric field, $\hat{V}(t) = -e\vec{E}(t) \cdot \vec{r}$, an effective Hamiltonian in the $|1\rangle$ and $|2\rangle$ subspace [when $\omega_r \approx \omega_Z$] can be written as:

$$\frac{\hat{H}_{\text{EFF}}^{12}}{\hbar} = \frac{1}{2} (\omega_r - \omega_Z + \Delta_Z^{12}) \hat{\sigma}_Z^{12} + \delta_+^{\text{EF}} \hat{\sigma}_+^{12} + \delta_-^{\text{EF}} \hat{\sigma}_-^{12} \quad (41)$$

where

$$\delta_{\pm}^{\text{EF}} = \frac{32m^*}{\pi^4 \hbar^3} \sum_{n=2}^{\infty} \frac{n^2 (1 + (-1)^n)}{(n^2 - 1)^3} \left(\frac{L_X^2 E_X \zeta_1(-\theta) \eta_X \exp(\pm i \phi_X)}{(n^2 - 1)^2 - \eta_X^2} - \frac{L_Y^2 E_Y \zeta_2(-\theta) \eta_Y \exp(\pm i \phi_Y)}{(n^2 - 1)^2 - \eta_Y^2} \right) \quad (42)$$

Like the case of modulating the size of the quantum dot, the effective Rabi frequency, $|\delta_{\pm}^{\text{EF}}|/(2\pi)$, is again proportional to the spin-orbit coupling strength. Figure 5(B) presents an exact numerical simulation of the transition amplitude, $|\langle 1, 1, + | T \exp(-i \int_0^t dt' \tilde{H}(t')/\hbar) | 1, 1, - \rangle|^2$, in the presence of an electric field, $\vec{E}(t) = E_X \sin(\omega_r t + \phi_X) \hat{x}$. The following parameters were used in the simulation: $L_X = L_Y = 70$ nm [giving $\hbar^2 \pi^2 / (2m^* L_{X(Y)}^2) \approx 1.1$ meV and $\eta_{X(Y)} = 0.087$], $E_X = 10^4$ eV/m, $\alpha = 4 \times 10^{-13}$ eV-m, $\beta = 0$ eV-m, $\hbar \omega_Z = 0.1$ meV, $\theta = 0$, and $(\omega_r - \omega_Z)/(2\pi) = -958.4$ kHz. Such parameters gave an effective Rabi frequency of 3.94 MHz, which is in excellent agreement with the calculated value given by Eq. (42), $|\delta_+^{\text{EF}}|/(2\pi) = 3.92$ MHz.

VI. PARAMETRIC ORBITAL AND SPIN EXCITATIONS FOR INCREASING SPIN POLARIZATION

In addition to single spin manipulations in parabolic quantum dots, combined transitions between both the spin and the orbital degrees of freedom can be generated under parametric modulation of $\hat{V}(\hat{X}, \hat{Y})$. In a parabolic quantum dot, application of an electric field [$\tilde{H}(t)$ in Eq. (25)] and/or modulation of ω_X and ω_Y [$\tilde{H}(t)$ in Eq. (20)] can directly induce both orbital and spin excitations. Such transitions are an essential component for proposals to increase spin polarization in a quantum dot's ground electronic state⁴⁰. Consider first the case of parametrically modulating a parabolic quantum dot's oscillator frequency, ω_X , in the absence of any static electric fields [$\tilde{H}(t)$ in Eq. (20) with $F_X = F_Y = 0$ eV/m]. In the following, we will neglect the cubic Dresselhaus interaction [\hat{H}_D^{cub} in Eq. (30)] and will take $\omega_Y > \omega_X$ in order that the parametric modulation can be chosen to connect states involving changes in only one of the orbital degrees of freedom, such as $|0, 0\rangle$ going to $|1, 0\rangle$. If we wish to generate transitions between the states $|1, 0, +\rangle$ and $|0, 0, -\rangle$, ω_X must be modulated at frequency of $\omega_r \approx \omega_X - \omega_Z$. Labeling the relevant states as $|2\rangle = |0, 0, -, 1_F\rangle$ and $|3\rangle = |1, 0, +, 0_F\rangle$, the effective Hamiltonian in the $\{|2\rangle, |3\rangle\}$ Floquet subspace under parametric modulation of ω_X (at $\omega_r \approx \omega_X - \omega_Z$) is given by:

$$\frac{\hat{H}_{\text{EFF}}^{23}}{\hbar} = \frac{1}{2} (\omega_Z - \omega_X + \omega_r + \Delta_Z^{23} + \delta_Z^{23}) \hat{\sigma}_Z^{23} + \delta_+^{23} \hat{\sigma}_+^{23} + \delta_-^{23} \hat{\sigma}_-^{23} \quad (43)$$

$$\begin{aligned} \Delta_Z^{23} &= \frac{m^* \omega_Z}{\hbar^3} \left(\frac{2\omega_X (\zeta_1(-\theta))^2}{\omega_Z^2 - \omega_X^2} + \frac{\omega_Y (\zeta_2(-\theta))^2}{\omega_Z^2 - \omega_Y^2} \right) \\ \delta_Z^{23} &\approx \frac{\delta \omega_X^2}{4\omega_X} \left(\frac{(\omega_X - \omega_Z)^2}{4\omega_X^2 - (\omega_X - \omega_Z)^2} \right) \\ \delta_{\pm}^{23} &= \sqrt{\frac{m\omega_X}{2\hbar^3}} \frac{\omega_Z \delta \omega_X \zeta_1(-\theta)}{\omega_X^2 - \omega_Z^2} \exp(\pm i \phi_X) \end{aligned} \quad (44)$$

By choosing $\omega_r = \omega_X - \omega_Z - \Delta_Z^{23} - \delta_Z^{23}$, efficient spin and orbital transitions between the states $|2\rangle$ and $|3\rangle$ can be generated [Fig. 6(A)] since the Rabi frequency, $|\delta_{\pm}^{23}|$, is directly proportional to the spin-orbit coupling. Note that there can be a significant Bloch-Siegert shift, δ_Z^{23} , since the transition involves different electronic orbitals.

Figure 6(A) presents an exact numerical simulation of the transition amplitudes, $|\langle 1, 0, + | T \exp(-i \int_0^t dt' \tilde{H}(t')/\hbar) | 0, 0, - \rangle|^2$ (black curve) and $|\langle 0, 0, + | T \exp(-i \int_0^t dt' \tilde{H}(t')/\hbar) | 0, 0, + \rangle|^2$ (red curve), in the presence of the modulation $\omega_X(t) = \omega_X + \delta\omega_X \sin(\omega_r t)$. The following parameters were used in the simulation: $\hbar\omega_Y = 1$ meV, $\hbar\omega_X = 0.25$ meV, $\alpha = 4 \times 10^{-13}$ eV-m, $\beta = 0$ eV-m, $\hbar\omega_Z = 0.1$ meV, $\theta = 0$, $F_X = F_Y = 0$ eV/m, and $\delta\omega_X = \omega_X/10$. Such parameters gave an effective Rabi frequency 48.1 MHz, which is in excellent agreement with the calculated value given by Eq. (44), $|\delta_{+}^{23}|/(2\pi) = 48.3$ MHz, under “on-resonant” modulation $[(\omega_r - (\omega_X - \omega_Z))/(2\pi) = 32.32$ MHz $-\delta_Z^{23}/(2\pi) = 17.35$ MHz]. Note that the state $|0, 0, +\rangle$ essentially does not evolve into any of the other states [the red line in Fig. 6(A)] thus confirming that the electron must be spin down in order to be excited from the state $|0, 0\rangle$. As mentioned earlier, such spin selective transitions can be used to increase the spin polarization of a quantum dot⁴⁰, which will be discussed later in this section.

Since the relevant transitions involve both orbital and spin excitation, the required modulation frequency is quite large, $\omega_r \approx \omega_X - \omega_Z \approx 36.3$ GHz, which can be experimentally challenging. However, higher-order processes which utilize smaller values of ω_r can be found in order to induce efficient spin and orbital transitions. The simplest higher-order process to induce transitions between the states $|1, 0, +\rangle$ and $|0, 0, -\rangle$ occurs when $\omega_r \approx (\omega_X - \omega_Z)/2$. In this case, the Floquet states $|1, 0, +, 0_F\rangle$ and $|0, 0, -, 2_F\rangle$ are degenerate. The effective Hamiltonian in this subspace is given by [for $\omega_r \approx (\omega_X - \omega_Z)/2$]:

$$\frac{\hat{H}_{2\omega}^{23}}{\hbar} = \frac{1}{2} (\omega_Z - \omega_X + 2\omega_r + \Delta_Z^{23} + \delta_{2\omega,Z}^{23}) \hat{\sigma}_Z^{23} + \delta_{2\omega,+}^{23} \hat{\sigma}_+^{23} + \delta_{2\omega,-}^{23} \hat{\sigma}_-^{23} \quad (45)$$

where

$$\begin{aligned} \delta_{2\omega,Z}^{23} &\approx \frac{\delta\omega_X^2}{4\omega_X} \left(\frac{(\omega_X - \omega_Z)^2}{16\omega_X^2 - (\omega_X - \omega_Z)^2} \right) \\ \delta_{2\omega,\pm}^{23} &= \mp i \sqrt{\frac{m^*}{32\omega_X \hbar^3}} \frac{(13\omega_X^2 + 2\omega_X\omega_Z + \omega_Z^2) \delta\omega_X^2 \zeta_1(-\theta)}{(\omega_X - \omega_Z)^2 (\omega_X + \omega_Z) (3\omega_X + \omega_Z)} \exp(\pm i 2\phi_X) \end{aligned} \quad (46)$$

In this case, the effective Rabi frequency is again directly proportional to the spin-orbit coupling strength and is also proportional to the square of the modulation strength, $(\delta\omega_X)^2$.

Figure 6(B) presents an exact numerical simulation of the transition amplitudes, $|\langle 1, 0, + | T \exp(-i \int_0^t dt' \tilde{H}(t')/\hbar) | 0, 0, - \rangle|^2$ (black curve) and $|\langle 0, 0, + | T \exp(-i \int_0^t dt' \tilde{H}(t')/\hbar) | 0, 0, + \rangle|^2$ (red curve), in the presence of modulating the oscillator frequency of the parabolic well at $\omega_r \approx (\omega_X - \omega_Z)/2$. The following parameters were used in the simulation: $\hbar\omega_Y = 1$ meV, $\hbar\omega_X = 0.25$ meV, $\alpha = 4 \times 10^{-13}$ eV-m, $\beta = 0$ eV-m, $\hbar\omega_Z = 0.1$ meV, $\theta = 0$, $\delta\omega_X = \omega_X/10$, and $(\omega_r - 1/2(\omega_X - \omega_Z))/(2\pi) = -\delta_{2\omega,Z}^{23}/(4\pi) + 16.16$ MHz = 14.42 MHz. The above parameters gave an effective Rabi frequency of 8.77 MHz, which is within 6% of the calculated value given by Eq. (46), $|\delta_{+}^{23}|/(2\pi) \approx 8.26$ MHz. Note also that the state $|0, 0, +\rangle$ doesn't evolve during the parametric modulation of ω_X [red curve in Fig. 6(B)].

In addition to modulating the confinement frequency, the spin-orbit coupling constants, α and β , can also be modulated in order to produce combined spin and orbital excitations which are first-order in α and β . By modulating an electric field generated by a surface gate above the quantum dot, the Rashba spin-orbit coupling parameter within the quantum dot can be controlled¹³; additionally, for quantum dots formed using semiconductor heterostructures, surface gates could also be used to change $\langle \hat{P}_Z^2 \rangle$ thereby changing the linear Dresselhaus coupling constant, $\beta = \gamma \langle \hat{P}_Z^2 \rangle$. Such modulations of the spin-orbit interaction have been previously suggested as a way to perform both spin and orbital excitations in the absence of a magnetic field¹⁴. Finally, it should be noted that application of an electric field can only couple the states $|1, 0, +\rangle$ and $|0, 0, -\rangle$ to second-order in the spin-orbit coupling for a parabolic quantum dot; therefore, the EDSR technique cannot generate such transitions as efficiently as modulating ω_X when the spin-orbit coupling is weak.

A. Increasing spin polarization in the lowest electronic orbital

Throughout this work, relaxation has been neglected when calculating the various spin transitions generated under parametric modulation of the quantum dot's electrostatic potential. In the previous sections where only effective spin rotations within the lowest electron state were considered, neglect of both T_1 and T_2 relaxation seemed justified since the calculated Rabi frequencies (1 – 30 MHz) were one to two orders of magnitude larger than the measured^{17,18,19,20} $1/T_1$ values in quantum dots (we assume that $1/T_2$ is on the same order⁴¹ as $1/T_1$). However, relaxation of excited electronic states in quantum dots occurs on the nanosecond time scale³, which is much faster than the calculated Rabi frequencies (order of 10 MHz) associated with combined spin and electronic excitation shown in Fig. 6; therefore, relaxation effects must be considered when examining such transitions.

The ability to coherently couple the states $|0, 0, -\rangle$ and $|1, 0, +\rangle$, coupled with relaxation, can be used to help spin polarize the electronic ground state of a quantum dot as depicted in Fig. 7(A). From Fig. 6, parametric modulation of the oscillator frequency can connect the state $|0, 0, -\rangle$ to the state $|1, 0, +\rangle$ while leaving the state $|0, 0, +\rangle$ relatively uncoupled from any other state of

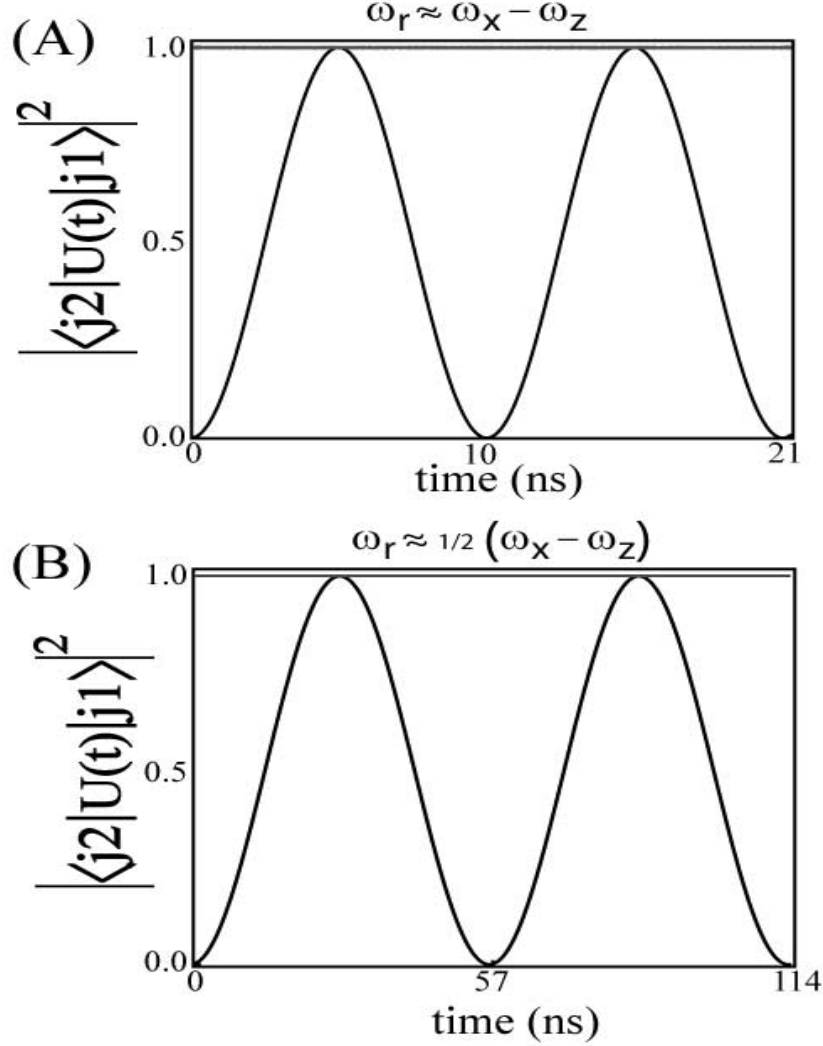


FIG. 6: (Color online) Numerical simulation of the transition amplitudes, $|\langle 0, 0, - | T \exp(-i \int_0^t dt' \tilde{H}(t')) | 1, 0, + \rangle|^2$ (black curve) and $|\langle 0, 0, + | T \exp(-i \int_0^t dt' \tilde{H}(t')) | 0, 0, + \rangle|^2$ (red curve) caused by modulating the oscillator strength defining the parabolic quantum dot, when (A) $\omega_r \approx \omega_X - \omega_Z$ and (B) $\omega_r \approx (\omega_X - \omega_Z)/2$. The following parameters were used in the simulations: $\hbar\omega_Y = 1$ meV, $\hbar\omega_X = 0.25$ meV, $\alpha = 4 \times 10^{-13}$ eV-m, $\beta = 0$ eV-m, $\hbar\omega_Z = 0.1$ meV, $\theta = 0$, $\delta\omega_X = \frac{\omega_X}{10}$, and $\phi_X = 0$. In (A), modulation of ω_X at a frequency of $\omega_r/(2\pi) \approx (\omega_X - \omega_Z)/(2\pi) = 36.3$ GHz can generate effective transitions between the states $|0, 0, -\rangle$ and $|1, 0, +\rangle$, which gave a Rabi frequency of 48.1 MHz, which is in excellent agreement with the calculated value given by Eq. (44), $|\delta_{+}^{23}|/(2\pi) = 48.3$ MHz. In (B), modulation of ω_X at a frequency of $\omega_r/(2\pi) \approx (\omega_X - \omega_Z)/(4\pi) = 18.15$ GHz resulted in a Rabi frequency of 8.77 MHz, which is within 6% of the calculated value given in Eq. (46), $|\delta_{2\omega, \pm}^{23}|/(2\pi) \approx 8.26$ MHz. Although the resulting Rabi frequency is smaller in Fig. 6(B) than in Fig. 6(A), the required ω_r is a factor of two smaller, which makes such modulations more experimentally feasible.

the quantum dot. An electron in the excited state $|1, 0, +\rangle$ can quickly relax to the state $|0, 0, +\rangle$ due to the direct coupling of the electron to piezo-phonons⁴², whereas the relaxation of the state $|1, 0, +\rangle$ to the state $|0, 0, -\rangle$, which requires an effective spin-phonon coupling, occurs at a much smaller rate. This differential relaxation can be used to generate spin polarization in the lowest electronic state in a manner similar to optical pumping⁴³ and Overhauser⁴⁴ techniques.

In the following work, the dynamics under parametric modulation of the confining potential has been restricted to the following subspace for simplicity: $\{|1\rangle \equiv |0, 0, +\rangle, |2\rangle \equiv |0, 0, -\rangle, |3\rangle \equiv |1, 0, +\rangle\}$, and the calculations were performed using different values of δ_{\pm}^{23} taken from the Fig. 6. The density matrix in this subspace can be written as $\rho(t) = \sum_{i=1}^3 p_{ii}(t)|i\rangle\langle i| + p_{23}(t)|2\rangle\langle 3| + p_{32}(t)|3\rangle\langle 2|$ (where only coherence between the states $|2\rangle$ and $|3\rangle$ have been considered). Defining W_{ij} to be the transition rate from state i to state j , and Γ_{23} to be the decoherence rate for the coherence between states

$|2\rangle$ and $|3\rangle$, the various coefficients in $\rho(t)$ can be found by solving:

$$\frac{d}{dt} \begin{pmatrix} p_{11} \\ p_{22} \\ p_{33} \\ p_{23} \\ p_{32} \end{pmatrix} = \begin{pmatrix} -(W_{12} + W_{13}) & W_{21} & W_{31} & 0 & 0 \\ W_{12} & -(W_{21} + W_{23}) & W_{32} & i\delta_{+}^{23} & -i\delta_{-}^{23} \\ W_{13} & W_{23} & -(W_{31} + W_{32}) & -i\delta_{+}^{23} & i\delta_{-}^{23} \\ 0 & i\delta_{-}^{23} & -i\delta_{+}^{23} & -\Gamma_{23} & 0 \\ 0 & -i\delta_{+}^{23} & i\delta_{-}^{23} & 0 & -\Gamma_{23} \end{pmatrix} \begin{pmatrix} p_{11} \\ p_{22} \\ p_{33} \\ p_{23} \\ p_{32} \end{pmatrix} \quad (47)$$

where the parametric modulation of the quantum dot is assumed not to affect the values of W_{ij} and Γ_{23} in Eq. (47). In the absence of any term connecting the states $|2\rangle$ and $|3\rangle$, i.e., $\delta_{\pm}^{23} = 0$, the various transition rates, W_{ij} , must satisfy the following conditions in order to ensure that the equilibrium density matrix, $\rho_{\text{eq}} = \sum_i p_{ii}^{\text{eq}} |i\rangle\langle i|$, is a solution to Eq. (47):

$$W_{ij} = \frac{p_{jj}^{\text{eq}}}{p_{ii}^{\text{eq}}} W_{ji} \quad (48)$$

where p_{jj}^{eq} is the equilibrium population for state j , with $p_{11}^{\text{eq}} > p_{22}^{\text{eq}} > p_{33}^{\text{eq}}$ and $\sum_i p_{ii}^{\text{eq}} = 1$.

In the presence of nonzero δ_{\pm}^{23} , the effective spin polarization of the ground electronic state, $P_Z = \frac{p_{11} - p_{22}}{p_{11} + p_{22}}$, can increase from its equilibrium value, $P_Z^{\text{eq}} = \frac{p_{11}^{\text{eq}} - p_{22}^{\text{eq}}}{p_{11}^{\text{eq}} + p_{22}^{\text{eq}}}$. Such an increase occurs since W_{31} involves only orbital relaxation, which is in general much faster than the transition rate W_{32} , which requires both orbital relaxation and a spin flip. Applying parametric modulations to the quantum dot can therefore transfer population from state $|2\rangle$ to state $|3\rangle$, which subsequently relaxes to state $|1\rangle$, thereby increasing the population difference between states $|1\rangle$ and $|2\rangle$. This is shown in Fig. 7(A).

The steady-state spin polarization under such parametric oscillations can be found by setting the left-hand side of Eq. (47) to zero and solving for p_{11} and p_{22} , which gives:

$$P_Z^{\text{steady-state}} = \frac{W_{31} \left(W_{13} + W_{23} + 2 \frac{|\delta_{\pm}^{23}|^2}{\Gamma_{23}} \right) + (W_{21} - W_{12} - W_{13}) \left(W_{31} + W_{32} + 2 \frac{|\delta_{\pm}^{23}|^2}{\Gamma_{23}} \right)}{W_{31} \left(W_{23} - W_{13} + 2 \frac{|\delta_{\pm}^{23}|^2}{\Gamma_{23}} \right) + (W_{21} + W_{12} + W_{13}) \left(W_{31} + W_{32} + 2 \frac{|\delta_{\pm}^{23}|^2}{\Gamma_{23}} \right)} \quad (49)$$

The transition rate, W_{31} , is mainly dominated by the coupling of the electron to piezo-phonons. From Eq. (4) of Ref.⁴⁵, this rate is given as $W_{31} \approx 3.74 \times 10^8 \text{ s}^{-1}$ (for $\hbar\omega_X = 0.25 \text{ meV}$ and $\hbar\omega_Y = 1 \text{ meV}$); using Eq. (7) of Ref.⁴⁵ as a rough estimate for W_{32} , one obtains $W_{32} \approx 5 \times 10^{-2} \text{ s}^{-1}$, which satisfies $W_{31} \gg W_{32}$. Although no theory has been attempted in this work to calculate Γ_{23} , as long as $2\Gamma_{23} \geq W_{31}$, the diagonal elements, p_{ii} , will be nonnegative (as seen from numerically integrating Eq. (47)). Although the value of Γ_{23} does not drastically affect $P_Z^{\text{steady-state}}$, it does affect the time scale in which $P_Z^{\text{steady-state}}$ is reached. In the following we simply take, for illustrative purposes, $\Gamma_{23} = 10W_{31}$. Finally, since the effective T_1 for GaAs quantum dots is on the order of milliseconds to microseconds^{17,18,19,20}, a conservative value of $T_1 = 100 \mu\text{s}$ was chosen, which provided the values of W_{12} and W_{21} from the condition that $1/T_1 = W_{12} + W_{21} = W_{21}(1 + \exp(\hbar\omega_Z/(k_B T)))$ [where the populations were assumed to be given by the Boltzmann distribution⁴⁶]. For $T = 2 \text{ K}$ and $\hbar\omega_Z = 0.1 \text{ meV}$, $W_{21} \approx 3.59 \times 10^3 \text{ s}^{-1}$. Using the parameters from Fig. 6(A) ($|\delta_{\pm}^{23}|/(2\pi) = 48.1 \text{ MHz}$), $P_Z(t)$ was found by integrating Eq. (47) and is shown (solid curve) in Fig. 7(B), with $P_Z^{\text{steady-state}} \approx 0.62 \approx 2.82P_Z^{\text{eq}}$, which is reached within $0.15 \mu\text{s}$. No oscillations are present in $P_Z(t)$ since $\Gamma_{23} \gg |\delta_{\pm}^{23}|$.

For the case of modulating ω_X at a frequency of $\omega_r \approx (\omega_X - \omega_Z)/2$ [with $|\delta_{2\omega_r, \pm}^{23}|/(2\pi) \approx 8.77 \text{ MHz}$ as shown in Fig. 6(B)], it took roughly twenty times as long ($\approx 3\mu\text{s}$) to reach $P_Z^{\text{steady-state}} \approx 0.62$, which is shown by the dashed curve in Fig. 7(B). It should be noted that $P_Z^{\text{steady-state}}$ is approximately equal to the initial equilibrium population difference between the states $|1\rangle$ and $|3\rangle$, $\frac{p_{11}^{\text{eq}} - p_{33}^{\text{eq}}}{p_{11}^{\text{eq}} + p_{33}^{\text{eq}}} \approx 0.62$. Thus turning on the coupling between $|2\rangle$ and $|3\rangle$ allows the initial ‘‘orbital’’ polarization between the states $|1\rangle$ and $|3\rangle$ to be transferred into spin polarization between the states $|1\rangle$ and $|2\rangle$. This process is similar to the Overhauser effect, where, by coupling the electron and nuclear spins, the initial electron spin polarization can be converted into nuclear polarization⁴⁴. Therefore, in order to increase $P_Z^{\text{steady-state}}$, experiments should be performed at low temperatures, large magnetic fields, and with increased lateral confinement, i.e., large ω_X . However, increasing ω_X requires modulating the quantum dot at a higher ω_r (which may be unfeasible experimentally) in addition to the fact that $|\delta_{\pm}^{23}|$ decreases with increasing ω_X , thereby increasing the time it takes to reach $P_Z^{\text{steady-state}}$.

Finally, it should be noted that the above calculations assumed that the quantum dot was isolated and absolutely closed from the leads, i.e., no electrons could enter or exit from the dot. However, if electrons are able to tunnel in/out of the quantum dot, modulating the electrostatic potential could be used to selectively ‘‘kick’’ out spin down electrons. ‘‘Re-zeroing’’ the state of the quantum dot to spin up could be used as an initialization step for a possible quantum computation^{19,40}. Such a process would require the tunneling rate out of the dot for an electron in state $|3\rangle$ to be much faster than W_{31} . However, the evolution under

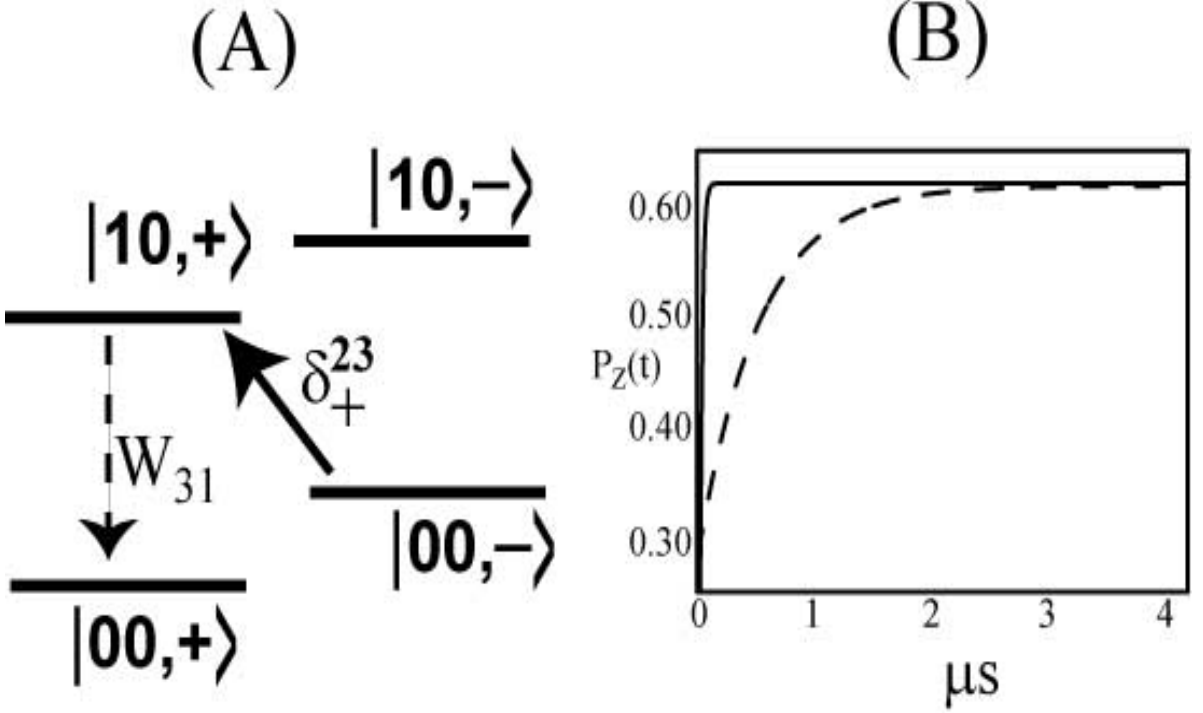


FIG. 7: Method for increasing the spin polarization of the lowest electronic state, $|0,0\rangle$. In (A), parametric modulations are performed in order to coherently connect the states $|2\rangle \equiv |0,0,-\rangle$ to the state $|3\rangle \equiv |1,0,+\rangle$ (which is denoted by δ_{\pm}^{23}), thereby transferring population from state $|2\rangle$ to state $|3\rangle$. The population in state $|3\rangle$ predominately relaxes to the state $|1\rangle \equiv |0,0,+\rangle$ due to the electron directly coupling to piezo-phonons, thereby increasing the spin polarization of the ground electronic state, $P_Z = \frac{p_{11} - p_{22}}{p_{11} + p_{22}}$. (B) Integration of Eq. (47) gave $P_Z(t)$ for parametric modulations of ω_X at the frequency $\omega_r = \omega_X - \omega_Z$ (solid curve) and at $\omega_r = (\omega_X - \omega_Z)/2$ (dashed curve). Along with the parameters used in Fig. 6, the following parameters were used in solving Eq. (47): $W_{31} = 3.74 \times 10^8 \text{ s}^{-1}$, $W_{32} = 5 \times 10^{-2} \text{ s}^{-1}$, $W_{21} = 3.59 \times 10^3 \text{ s}^{-1}$, $T = 2 \text{ K}$, $\Gamma_{23} = 10W_{31}$, and $|\delta_{\pm}^{23}|/(2\pi) \approx 48.1 \text{ MHz}$ (solid curve) and $|\delta_{\pm}^{23}|/(2\pi) \approx 8.77 \text{ MHz}$ (dashed curve). In both cases, $P_Z^{\text{steady-state}} \approx 0.62$ [Eq. (49)], although for larger $|\delta_{\pm}^{23}|$, $P_Z^{\text{steady-state}}$ was reached on a faster time scale [$0.15 \mu\text{s}$ (solid curve) compared to $3 \mu\text{s}$ (dashed curve)].

parametric modulations of the confining potential would have to be reconsidered, since in the case of a non-isolated quantum dot, there would be a finite probability during the parametric modulation that an electron in the state $|1\rangle$ would get excited and kicked out of the dot if the tunneling rate out of the dot is very large.

VII. DISCUSSION AND CONCLUSIONS

In this work, a general formalism combining Floquet theory with effective Hamiltonian theory was used to study the spin dynamics under parametric modulations of a lateral quantum dot's electrostatic potential in the presence of spin-orbit coupling. In parabolic quantum dots, modulating the center of the quantum dot, i.e., performing an EDSR experiment, was found to generate larger Rabi frequencies than parametrically modulating the confining frequency (in the absence of static electric fields), since the latter is second-order in spin-orbit coupling. However, in the presence of a static electric field, both methods gave similar Rabi frequencies for a parabolic quantum dot. For square dots, both EDSR and modulating the width/length of the quantum dot generate Rabi frequencies which are first-order in spin-orbit coupling. The modulation frequency must be chosen with precision on the order of the Rabi frequency (on the order of tens of MHz) in order to maximize the amplitude of the Rabi oscillations, thereby providing better spectroscopic precision of the quantum dot's energy levels relative to transport measurements, where thermal effects decrease the spectral resolution.

Inclusion of the cubic Dresselhaus spin-orbit coupling didn't dramatically alter the results obtained for parametric modulation in a parabolic quantum dot. However, the cubic Dresselhaus interaction tends to decrease the contribution of the linear Dresselhaus interaction to the Rabi frequency. Furthermore, measurement of the Rabi frequency under, for example, an EDSR

experiment using different orientations of the in-plane magnetic field could be used to determine the ratio of the Rashba spin-orbit coupling constant to the difference of the linear Dresselhaus spin-orbit coupling constant with the product of the cubic Dresselhaus coupling constant and the oscillator frequency (ω_X or ω_Y). For example, using Eq. (29) and including the cubic Dresselhaus coupling from Eq. (32) gives:

$$ZZ\left(\frac{\pi}{2}\right) = \frac{\beta - \frac{m^* \omega_Y \gamma}{2\hbar}}{\alpha} \quad (50)$$

In order to separate γ from β in Eq. (50), experiments could be repeated for different values of ω_Y , which would leave the linear Dresselhaus's contribution to $ZZ(\pi/2)$ unchanged but would alter the cubic Dresselhaus's contribution. Alternatively, it was shown that applying a time-dependent electric field along the \hat{y} direction coupled with parametric modulation of the confinement frequency along the \hat{x} direction could be used to generate Rabi frequencies which were proportional to γ and were independent of α and β to first-order. Measurement of the resulting Rabi frequency would provide another independent measure of the cubic Dresselhaus spin-orbit coupling constant.

Parametric modulations of the confining potential were also shown to generate combined spin and orbital excitations in a parabolic quantum dot with Rabi frequencies on the order of tens of MHz. However, since electronic relaxation times are on the order of nanoseconds, the effects of orbital relaxation had to be taken into account. A combination of coherent spin and orbital excitation with orbital relaxation was shown to be able to increase the spin polarization of the ground electronic state [Fig. 7] by transferring the initial "electronic polarization" between the ground and excited electronic state into spin polarization of the ground state. For the parameters chosen in this work, this corresponded to a three-fold increase in the spin polarization of the ground electronic state. Larger spin polarizations could be achieved by either using a more confined quantum dot (larger ω_X), larger magnetic fields, or by going to lower temperatures.

Finally, the spin control developed in this work used only parametric modulations of idealized electrostatic potentials (parabolic and square-box), which should only be considered as a model for spin control in lateral quantum dots. For such methods to be used in actual experimental quantum dots, more realistic electrostatic potentials³¹ for a quantum dot, i.e., non-parabolic and non-square-box potentials, are required. Furthermore, additional work is needed in order to better characterize the actual time-dependent electrostatic potentials generated by modulating the surface gate voltages of the quantum dot along with designing optimal configurations of surface gates in order to generate a desired transition. The results presented in this work could furthermore be extended to many-electron quantum dots, where the effects of electron-electron coupling on performing spin excitations should be examined. Recent theoretical work⁴⁷ has demonstrated that electronically controlled, magnetic dipole-like couplings between spins in different quantum dots can also be generated. These couplings, along with single spin rotations, could be used to generate multiple-quantum coherences between the electrons in different quantum dots by completely electrostatic means. In addition to being used to better characterize the electron-environment coupling of such highly correlated states, generating such highly correlated states could be used as an intermediary step during a quantum computation.

Acknowledgments

We would like to thank Prof. Eric Heller and Prof. Yung-Ya Lin for their support. This work was supported by NSF (CHE-0349362 and CHE-0116853).

* Electronic address: jwalls@fas.harvard.edu

¹ D. Loss and D.P. DiVincenzo, Phys. Rev. A **57**, 120 (1998).

² F.H.L. Koppens, C. Buizert, K.J. Tielrooij, I.T. Vink, K.C. Nowack, T. Meunier, L.P. Kouwenhoven, and L.M.K. Vandersypen, Nature **442**, 766 (2006).

³ J.R. Petta, A.C. Johnson, C.M. Marcus, M.P. Hanson, and A.C. Gossard, Phys. Rev. Lett. **93**, 186802 (2004).

⁴ J.R. Petta, A.C. Johnson, J.M. Taylor, E.A. Laird, A. Yacoby, M.D. Lukin, C.M. Marcus, M.P. Hanson, and A.C. Gossard, Science **309**, 2180 (2005).

⁵ G. Salis, Y. Kato, K. Ensslin, D.C. Driscoll, A.C. Gossard, and D.D. Awschalom, Nature **414**, 619 (2001).

⁶ Y. Kato, R.C. Meyers, D.C. Driscoll, A.C. Gossard, J. Levy, and D.D. Awschalom, Science **299**, 1201 (2003).

⁷ Y. Tokura, W.G. vanderWiel, T. Obata, and S. Tarucha, Phys. Rev. Lett. **96**, 047202 (2006).

⁸ E.I. Rashba and A.L. Efros, Appl. Phys. Lett. **83**, 5295 (2003).

⁹ E.I. Rashba and A.L. Efros, Phys. Rev. Lett. **91**, 126405 (2003).

¹⁰ A.L. Efros and E.I. Rashba, Phys. Rev. B **73**, 165325 (2006).

¹¹ V.N. Golovach, M. Borhani, and D. Loss, Phys. Rev. B **74**, 165319 (2006).

¹² C. Flindt, A.S. Sorensen, and K. Flensberg, Phys. Rev. Lett. **97**, 240501 (2006).

¹³ J. Nitta, T. Akazaki, H. Takayanagi, and T. Enoki, Phys. Rev. Lett. **78**, 1335 (1997).

- ¹⁴ S. DeBald and C. Emary, Phys. Rev. Lett. **94**, 226803 (2005).
¹⁵ H.A. Engel and D. Loss, Phys. Rev. Lett. **86**, 4648 (2001).
¹⁶ H.A. Engel and D. Loss, Phys. Rev. B **65**, 195321 (2002).
¹⁷ T. Fujisawa, D.G. Austing, Y. Tokura, Y. Hirayama, and S. Tarucha, Nature **419**, 278 (2002).
¹⁸ R. Hanson, B. Witkamp, L.M.K. Vandersypen, L.H.W. van Beveren, J.M. Elzerman, and L.P. Kouwenhoven, Phys. Rev. Lett. **91**, 196802 (2003).
¹⁹ J.M. Elzerman, R. Hanson, L.H. Willems van Beveren, B. Witkamp, L.M.K. Vandersypen, and L.P. Kouwenhoven, Nature **430**, 431 (2004).
²⁰ S. Amasha, K. Maclean, I. Radu, D.M. Zumbuhl, M.A. Kastner, M.P. Hanson, and A.C. Gossard, cond-mat/060711 (2006).
²¹ J.J. Sakurai, *Modern Quantum Mechanics* (Addison Wesley, New York, 1994).
²² J.H. Shirley, Phys. Rev. B **979** (1965).
²³ I. Shavitt and L.T. Redmon, J. Chem. Phys. **73**, 5711 (1980).
²⁴ C. Cohen-Tannoudji, J. Dupont-Roc, and G. Grynberg, *Atom-photon Interactions* (Wiley Science, New York, 1992).
²⁵ Y.A. Bychkov and E.I. Rashba, J. Phys. C **17**, 6039 (1984).
²⁶ G. Dresselhaus, Phys. Rev. **100**, 580 (1955).
²⁷ S. Tarucha, D.G. Austing, T. Honda, R.J. van der Hage, and L.P. Kouwenhoven, Phys. Rev. Lett. **77**, 3613 (1996).
²⁸ P.A. Maksym and T. Chakraborty, Phys. Rev. Lett. **65**, 108 (1990).
²⁹ U. Merkt, J. Huser, and M. Wagner, Phys. Rev. B **43**, 7320 (1991).
³⁰ F. Bloch and A. Siegert, Phys. Rev. **57**, 522 (1940).
³¹ M. Stopa, Phys. Rev. B **54**, 13767 (1996).
³² J.J. Krich and B.I. Halperin, cond-mat/0702667 (2007).
³³ E. Rasanen, H. Saarikoski, V.N. Stavrou, A. Harju, M.J. Puska, and R.M. Nieminen, Phys. Rev. B **67**, 235307 (2003).
³⁴ G.W. Bryant, Phys. Rev. Lett. **59**, 1140 (1987).
³⁵ S. Tomsovic and E.J. Heller, Phys. Rev. Lett. **67**, 664 (1991).
³⁶ C.M. Marcus, R.M. Westervelt, P.F. Hopkins, and A.C. Gossard, Phys. Rev. B **48**, 2460 (1993).
³⁷ P. Seba, Phys. Rev. A **41**, 2306 (1990).
³⁸ M. Razavy, Phys. Rev. A **44**, 2384 (1991).
³⁹ D. Cohen, A. Barnett, and E.J. Heller, Phys. Rev. E **63**, 046207 (2001).
⁴⁰ M. Friesen, C. Tahan, R. Joynt, and M.A. Eriksson, Phys. Rev. Lett. **92**, 037901 (2004).
⁴¹ V.N. Golovach, A. Khaetskii, and D. Loss, Phys. Rev. Lett. **93**, 016601 (2004).
⁴² A.V. Khaetskii and Y.V. Nazarov, Phys. Rev. B **64**, 125316 (2001).
⁴³ W. Happer, Rev. Mod. Phys. **44**, 169 (1972).
⁴⁴ C.P. Slichter, *Principles of Magnetic Resonance* (Springer, New York, 1996).
⁴⁵ A.V. Khaetskii and Y.V. Nazarov, Phys. Rev. B **61**, 12639 (2000).
⁴⁶ C.W.J. Beenakker, Phys. Rev. B **44**, 1646 (1991).
⁴⁷ M. Trif, V.N. Golovach, and D. Loss, Phys. Rev. B **75**, 085307 (2007).

APPENDIX A: THE EFFECTIVE HAMILTONIAN

If for a given Hamiltonian (written for convenience in Floquet space), $\hat{H}_F = \hat{H}_F^0 + \hat{V}_F$, there exists a subspace of interest, Q , which is weakly coupled by \hat{V}_F to the rest of the Floquet space, U , then the dynamics within Q can be separated from U by constructing an effective Hamiltonian from $\hat{H}_F, \hat{H}_F^{\text{EFF}}$, which is block-diagonal in the Q and U subspaces^{23,24}. Defining \hat{P}_Q to be the projection operator onto the subspace Q , $\hat{P}_Q = \sum_{|\alpha, m_F\rangle \in Q} |\alpha, m_F\rangle \langle \alpha, m_F|$, and \hat{P}_U to be the complementary projection operator onto the subspace U , $\hat{P}_U = \hat{1}_F - \hat{P}_Q$, \hat{H}_F^{EFF} can be determined by constructing a unitary transformation, $\exp(\hat{S}_F)$, such that $\exp(\hat{S}_F) \hat{H}_F \exp(-\hat{S}_F) = \hat{H}_F^{\text{EFF}}$, where in order to ensure that \hat{H}_F^{EFF} is block diagonal in both the Q and U subspaces, \hat{H}_F^{EFF} must satisfy the following:

$$\hat{P}_Q \hat{H}_F^{\text{EFF}} \hat{P}_U = \hat{P}_U \hat{H}_F^{\text{EFF}} \hat{P}_Q = \hat{0} \quad (\text{A1})$$

Using Eq. (A1), a perturbation expansion for \hat{S}_F in powers of \hat{V}_F , $\hat{S}_F = \sum_{m=1}^{\infty} \hat{S}_F^{(m)}$, can be constructed. Separating \hat{V}_F into its diagonal and off-diagonal components, $\hat{V}_F = \hat{V}_F^S + \hat{V}_F^D$, with $\hat{V}_F^S = \hat{P}_Q \hat{V}_F \hat{P}_U + \hat{P}_U \hat{V}_F \hat{P}_Q$ and $\hat{V}_F^D = \hat{P}_U \hat{V}_F \hat{P}_U + \hat{P}_Q \hat{V}_F \hat{P}_Q$, \hat{S}_F can be written up to $m = 3$ as:

$$\begin{aligned} \langle \alpha, m_F | \hat{S}_F^{(1)} | \beta, n_F \rangle &= \frac{\langle \alpha, m_F | \hat{V}_F^S | \beta, n_F \rangle}{E_\alpha - E_\beta + \hbar(m-n)\omega_r} \\ \langle \alpha, m_F | \hat{S}_F^{(2)} | \beta, n_F \rangle &= \frac{\langle \alpha, m_F | [\hat{S}_F^{(1)}, \hat{V}_F^D] | \beta, n_F \rangle}{E_\alpha - E_\beta + \hbar(m-n)\omega_r} \\ \langle \alpha, m_F | \hat{S}_F^{(3)} | \beta, n_F \rangle &= \frac{\langle \alpha, m_F | [\hat{S}_F^{(2)}, \hat{V}_F^D] | \beta, n_F \rangle}{E_\alpha - E_\beta + \hbar(m-n)\omega_r} + \frac{\langle \alpha, m_F | [\hat{S}_F^{(1)}, [\hat{S}_F^{(1)}, \hat{V}_F^S]] | \beta, n_F \rangle}{3(E_\alpha - E_\beta + \hbar(m-n)\omega_r)} \end{aligned} \quad (\text{A2})$$

Using the above values of \widehat{S}_F in Eq. (A2), the effective Hamiltonian in the subspace Q , $\widehat{P}_Q \widehat{H}_F^{\text{EFF}} \widehat{P}_Q = \sum_{m=0}^{\infty} \widehat{H}_F^{\text{EFF}(m)}$, is given (up to order $(\widehat{V}_F)^4$) as:

$$\begin{aligned}
\langle \alpha_1, n_F | \widehat{H}_F^{\text{EFF}(0)} | \alpha_2, m_F \rangle &= \langle \alpha_1, n_F | \widehat{H}_F^0 | \alpha_2, m_F \rangle \\
\langle \alpha_1, n_F | \widehat{H}_F^{\text{EFF}(1)} | \alpha_2, m_F \rangle &= \langle \alpha_1, n_F | \widehat{V}_F^D | \alpha_2, m_F \rangle \\
\langle \alpha_1, n_F | \widehat{H}_F^{\text{EFF}(2)} | \alpha_2, m_F \rangle &= \frac{1}{2} \langle \alpha_1, n_F | [\widehat{S}_F^{(1)}, \widehat{V}_F^S] | \alpha_2, m_F \rangle \\
\langle \alpha_1, n_F | \widehat{H}_F^{\text{EFF}(3)} | \alpha_2, m_F \rangle &= \frac{1}{2} \langle \alpha_1, n_F | [\widehat{S}_F^{(2)}, \widehat{V}_F^S] | \alpha_2, m_F \rangle \\
\langle \alpha_1, n_F | \widehat{H}_F^{\text{EFF}(4)} | \alpha_2, m_F \rangle &= \frac{1}{2} \langle \alpha_1, n_F | [\widehat{S}_F^{(3)}, \widehat{V}_F^S] | \alpha_2, m_F \rangle - \frac{1}{24} \langle \alpha_1, n_F | [\widehat{S}_F^{(1)}, [\widehat{S}_F^{(1)}, [\widehat{S}_F^{(1)}, \widehat{V}_F^S]]] | \alpha_2, m_F \rangle
\end{aligned} \tag{A3}$$